ments, the position of probe in the nucleus accumbens was confirmed in all mice. The DA levels in each fraction were measured by high performance liquid chromatography (HPLC), with electrochemical detection using a reversed phase column (EICOMPAK PP-ODS, 4.6×30 mm, Eicom, Kyoto, Japan) and a mobile phase 1% MeOH/100 mM phosphate buffer (pH 6.0) including 50 mg/L disodium EDTA disodium and 500 mg/L sodium decane-1-sulfonate.

Conditioned Place Preference (CPP)

The place conditioning paradigm (CPP; Brain Science Idea Inc., Osaka, Japan) was used to study METH-induced rewarding effects, as reported previously [49]. Mice were allowed to move freely between transparent and black compartments for 15 min, once a day, for 3 days (days 1–3), as preconditioning. On day 3, the time spent in each compartment was measured. There was no significant difference between time spent in the black compartment with a smooth floor and the time spent in the transparent compartment with a textured floor, indicating that mice had no compartment preference before conditioning. On days 4, 6, and 8, mice were administered either vehicle (10 ml/kg, s.c.) or METH (1.0 mg/kg, s.c.), and then confined in either the transparent or black compartment for 30 min. On days 5, 7, and 9, the mice were given vehicle and placed in the non- METH assigned compartment, for 30 min. On day 10, the post-conditioning test was performed without drug treatment, and the time individual mice spent in each compartment was measured for 15 min. A counterbalanced protocol was used in order to nullify the initial preference of each mouse. The CPP score was designated as the time spent in the drug-conditioning sites minus the time spent in the saline-conditioning sites.

Western Blot Analysis

In a preliminary experiment, we examined the time course for phosphorylation of ERK1/2 in the striatum, after a single dose of METH (3 mg/kg). We found increased phosphorylation of ERK1/2 15 min after a single METH administration (data not shown), consistent with a previous result [50]. In further experiments, mice were therefore sacrificed 15 min after dosing with either saline (10 ml/kg) or METH (3 mg/kg), then, the striatum, frontal cortex and hippocampus were dissected out on ice. Briefly, striatum from individual mice were frozen and homogenized in 500 µl of lysis buffer (20 mM TBS, pH 7.6, 10 mM NaF, 1 mM Na_3VO_4, 1% Triton x-100, 5 mM EDTA, 5 mM EGTA containing protease inhibitor) using a Polytron homogenizer. The sample was left to stand on ice for 30 min and then centrifuged at 10,000× g and 4°C for 30 min. Total protein in the supernatant was measured using the DC protein assay (Bio-Rad, Hercules, CA). The sample was then diluted with 5× SDS sample buffer (62.5 mM Tris-HCl, pH 6.8, 10% glycerol, 2% SDS, 5% β-mercaptoethanol and bromophenol blue). Aliquots (10 µg protein) of protein were incubated for 5 min at 95°C, then separated using SDS-PAGE on 12% polyacrylamide gels. Proteins were transferred for 1 h onto a polyvinylidene difluoride (PVDF) membrane (GE Healthcare Amersham Hybond™-P, UK), using Trans Blot Mini Cell apparatus (Bio-Rad, Hercules, CA). The transfer buffer consisted of 25 mM Tris and 192 mM glycine. After protein transfer, membranes were blocked for 45 min in TBS-T (20 mM Tris-HCl, pH 7.6, 137 mM NaCl, 0.1% Tween-20) containing 5% skimmed milk at RT, followed by incubation with anti-rabbit P44/42-ERK antibody (1:1000, Cell Signaling, Cambridge, MA), overnight at 4°C in TBS-T, containing 5% BSA. After three washes in TBS-T, membranes were incubated with secondary antibody (1:15,000) in TBS-T for 1 h at RT. After repeated washes, protein bands were detected using the ECL chemiluminescence detection system (GE Healthcare Bioscience, UK). Images were captured using a Fuji LAS3000-mini imaging system (Fujifilm, Tokyo, Japan), and chemiluminescence bands were quantified. To calculate the amount of phosphorylated protein relative to total protein, membranes were stripped in buffer (100 mM 2-mercaptoethanol, 2% SDS, and 62.5 mM Tris-HCl, pH 6.7) at 60°C for 30 min, washed, blocked, re-incubated with rabbit anti-ERK (1:1000, Cell signaling, Cambridge, MA), and detected as described above.

Statistical Analysis

All data were expressed as a mean ± standard error of the mean (S.E.M.). The behavior data, CPP score and ERK expression data were analyzed by two-way ANOVA (genotype vs. drug treatment). Student's t-test and one-way analysis of variance (ANOVA), followed Bonferroni/Dunn test were used for comparison between the two groups and comparison of multiple groups, respectively. The results of extracellular DA levels were analyzed by repeated one-way ANOVA, followed by the student's *t*-test. Values of $p<0.05$ were regarded as statistically significant.

Supporting Information

Figure S1 Effect of pretreatment with D-serine on acute hyperlocomotion after a single dose of METH. Thirty minutes after a single oral dose of vehicle (10 ml/kg) or D-serine (900 mg/kg), WT and *Srr*-KO mice were given a dose of METH (3 mg/kg, s.c.). Behavioral evaluation of locomotion was performed 2 hours after the dose of METH, as described in the Methods and Materials section. Each value is the mean ± SEM (n = 7 per group). NS: Not significant (Student's t-test).
(TIFF)

Figure S2 Effects of pretreatment with D-serine on behavioral sensitization after repeated administration of METH. Thirty minutes after a single oral administration of vehicle (10 ml/kg) or D-serine (900 mg/kg), WT and *Srr*-KO mice were dosed with METH (3 mg/kg) for 5 consecutive days. Seven days after the final dose of METH, a lower dose of METH (1 mg/kg, s.c.) was administered to all mice. Behavioral evaluation of locomotion was performed. Each value is the mean ± SEM (n = 7 per group). ***$p<0.01$ as compared with the vehicle treated group (Bonferroni/Dunn method). NS: Not significant (Student's t-test).
(TIFF)

Figure S3 Phosphorylation of ERK1/2 in the hippocampus after a single dose of METH. Mice were sacrificed 15 minutes after a single dose of either METH (3 mg/kg, s.c.) or vehicle (10 ml/kg, s.c.). Western blot analysis of phospho-ERK1/2 and total ERK1/2 protein was performed as described in the Methods and Materials. Values are the mean ± S.E.M. (n = 6 per group).
(TIFF)

Table S1 [^{3}H](+)-MK-801 binding to mouse brain regions. Binding of [^{3}H](+)-MK-801 (3 nM; 1.02 TBq/mmol, PerkinElmer, MA, USA) to the crude membranes from brain regions (frontal cortex, hippocampus, striatum, cerebellum) was performed. Non-specific binding was determined in the presence of 10 µM of (+)-MK-801. There were no differences between WT mice and *Srr*-KO mice. Values are the mean ± S.E.M. (n = 7 per group).
(DOCX)

Acknowledgments

Mao Horio was supported by Ishidsu Shun Memorial Scholarship, Japan. We would like to thank Professor Masaomi Iyo (Department of Psychiatry, Chiba University Graduate School of Medicine) for his support.

Author Contributions

Conceived and designed the experiments: KH. Performed the experiments: MH MK YF TI. Analyzed the data: MH KH. Contributed reagents/materials/analysis tools: RI HM. Wrote the paper: MH KH.

References

1. Hashimoto K (2007) Chapter 1.*New Research on methamphetamine abuse.* In Toolancy GH, ed. Nova Science Publishers, Inc, New York. pp 1–51.
2. Gonzales R, Mooney L, Rawson RA (2010) The methamphetamine problem in the united states. Annu Rev Public Health 31: 385–398.
3. Sato M, Chen CC, Akiyama K, Otsuki S (1983) Acute exacerbation of paranoid psychotic state after long-term abstinence in patients with previous methamphetamine psychosis. Biol Psychiatry 18: 429–440.
4. Ujike H, Sato M (2004) Clinical features of sensitization to methamphetamine observed in patients with methamphetamine dependence and psychosis. Ann N Y Acad Sci 1025: 279–287.
5. Featherstone RE, Kapur S, Fletcher PJ (2007) The amphetamine-induced sensitized state as a model of schizophrenia. Prog Neuropsychopharmacol Biol Psychiatry 31: 1556–1571.
6. Chen H, Wu J, Zhang J, Hashimoto K (2010) Recent topics on pharmacotherapy for amphetamine-type stimulants abuse and dependence. Curr Drug Abuse Rev 3: 222–238.
7. Karila L, Weinstein A, Aubin HJ, Benyamina A, Reynaud M, et al. (2010) Pharmacological approaches to methamphetamine dependence: A focused review. Br J Clin Pharmacol 69: 578–592.
8. Cadet JL, Jayanthi S, Deng X (2003) Speed kills: Cellular and molecular bases of methamphetamine-induced nerve terminal degeneration and neuronal apoptosis. FASEB J 17: 1775–1788.
9. Tata DA, Yamamoto BK (2007) Interactions between methamphetamine and environmental stress: Role of oxidative stress, glutamate and mitochondrial dysfunction. Addiction 102(Suppl 1): 49–60.
10. Earle ML, Davies JA (1991) The effect of methamphetamine on the release of glutamate from striatal slices. J Neural Transm Gen Sect 86: 217–222.
11. O'Dell SJ, Weihmuller FB, Marshall JF (1991) Multiple methamphetamine injections induce marked increases in extracellular striatal dopamine which correlate with subsequent neurotoxicity. Brain Res 564: 256–260.
12. Segal DS, Kuczenski R (1997) Repeated binge exposures to amphetamine and methamphetamine: Behavioral and neurochemical characterization. J Pharmacol Exp Ther 282: 561–573.
13. Chen JC, Liang KW, Huang YK, Liang CS, Chiang YC (2001) Significance of glutamate and dopamine neurons in the ventral pallidum in the expression of behavioral sensitization to amphetamine. Life Sci 68: 973–983.
14. Robinson TE, Becker JB (1986) Enduring changes in brain and behavior produced by chronic amphetamine administration: A review and evaluation of animal models of amphetamine psychosis. Brain Res 396: 157–198.
15. Pierce RC, Kalivas PW (1997) A circuitry model of the expression of behavioral sensitization to amphetamine-like psychostimulants. Brain Res Brain Res Rev 25: 192–216.
16. Karler R, Calder LD, Turkanis SA (1991) DNQX blockade of amphetamine behavioral sensitization. Brain Res 552: 295–300.
17. Wolf ME, Khansa MR (1991) Repeated administration of MK-801 produces sensitization to its own locomotor stimulant effects but blocks sensitization to amphetamine. Brain Res 562: 164–168.
18. Ohmori T, Abekawa T, Muraki A, Koyama T (1994) Competitive and noncompetitive NMDA antagonists block sensitization to methamphetamine. Pharmacol Biochem Behav 48: 587–591.
19. Kuribara H, Asami T, Ida I, Iijima Y, Tadokoro S (1992) Effects of repeated MK-801 on ambulation in mice and in sensitization following methamphetamine. Psychopharmacology (Berl) 108: 271–275.
20. Kim HS, Jang CG (1997) MK-801 inhibits methamphetamine-induced conditioned place preference and behavioral sensitization to apomorphine in mice. Brain Res Bull 44: 221–227.
21. Schell MJ (2004) The N-methyl D-aspartate receptor glycine site and D-serine metabolism: An evolutionary perspective. Philos Trans R Soc Lond B Biol Sci 359: 943–964.
22. Martineau M, Baux G, Mothet JP (2006) D-serine signalling in the brain: Friend and foe. Trends Neurosci 29: 481–491.
23. Wolosker H (2007) NMDA receptor regulation by D-serine: New findings and perspectives. Mol Neurobiol 36: 152–164.
24. Wolosker H, Blackshaw S, Snyder SH (1999) Serine racemase: A glial enzyme synthesizing D-serine to regulate glutamate-N-methyl-D-aspartate neurotransmission. Proc Natl Acad Sci U S A 96: 13409–13414.
25. Wolosker H, Sheth KN, Takahashi M, Mothet JP, Brady RO, Jr., et al. (1999) Purification of serine racemase: Biosynthesis of the neuromodulator D-serine. Proc Natl Acad Sci U S A 96: 721–725.
26. Miya K, Inoue R, Takata Y, Abe M, Natsume R, et al. (2008) Serine racemase is predominantly localized in neurons in mouse brain. J Comp Neurol 510: 641–654.
27. Inoue R, Hashimoto K, Harai T, Mori H (2008) NMDA- and beta-amyloid$_{1-42}$-induced neurotoxicity is attenuated in serine racemase knock-out mice. J Neurosci 28: 14486–14491.
28. Basu AC, Tsai GE, Ma CL, Ehmsen JT, Mustafa AK, et al. (2009) Targeted disruption of serine racemase affects glutamatergic neurotransmission and behavior. Mol Psychiatry 14: 719–727.
29. Horio M, Kohno M, Fujita Y, Ishima T, Inoue R, et al. (2011) Levels of D-serine in the brain and peripheral organs of serine racemase (*srr*) knock-out mice. Neurochem Int 59: 853–859.
30. Rajadhyaksha A, Husson I, Satpute SS, Kuppenbender KD, Ren JQ, et al. (2004) L-type Ca^{2+} channels mediate adaptation of extracellular signal-regulated kinase 1/2 phosphorylation in the ventral tegmental area after chronic amphetamine treatment. J Neurosci 24: 7464–7476.
31. Valjent E, Pascoli V, Svenningsson P, Paul S, Enslen H, et al. (2005) Regulation of a protein phosphatase cascade allows convergent dopamine and glutamate signals to activate ERK in the striatum. Proc Natl Acad Sci U S A 102: 491–496.
32. Pierce RC, Kalivas PW (1997) A circuitry model of the expression of behavioral sensitization to amphetamine-like psychostimulants. Brain Res Rev 25: 192–216.
33. Vanderschuren LJMJ, Kalivas PW (2000) Alterations in dopaminergic and glutamatergic transmission in the induction and expression of behavioral sensitization: a critical review of preclinical studies. Psychopharmacology 151: 99–120.
34. Berke JD, Hyman SE (2000) Addiction, dopamine, and the molecular mechanisms of memory. Neuron 25: 515–532.
35. Chao J, Nestler EJ (2004) Molecular neurobiology of drug addiction. Annu Rev Med 55: 113–132.
36. Girault JA, Valjent E, Caboche J, Herve D (2007) ERK2: A logical AND gate critical for drug-induced plasticity? Curr Opin Pharmacol 7: 77–85.
37. Zhai H, Li Y, Wang X, Lu L (2008) Drug-induced alterations in the extracellular signal-regulated kinase (ERK) signalling pathway: Implications for reinforcement and reinstatement. Cell Mol Neurobiol 28: 157–172.
38. Mizoguchi H, Yamada K, Mizuno M, Mizuno T, Nitta A, et al. (2004) Regulations of methamphetamine reward by extracellular signal-regulated kinase 1/2/ets-like gene-1 signaling pathway via the activation of dopamine receptors. Mol Pharmacol 65: 1293–1301.
39. Valjent E, Corvol JC, Trzaskos JM, Girault JA, Herve D (2006) Role of the ERK pathway in psychostimulant-induced locomotor sensitization. BMC Neurosci 7: 20.
40. Gerfen CR, Paletzki R, Worley P (2008) Differences between dorsal and ventral striatum in Drd1a dopamine receptor coupling of dopamine- and cAMP-regulated phosphoprotein-32 to activation of extracellular signal-regulated kinase. J Neurosci 28: 7113–7120.
41. Bertran-Gonzalez J, Bosch C, Maroteaux M, Matamales M, Herve D, et al. (2008) Opposing patterns of signaling activation in dopamine D_1 and D_2 receptor-expressing striatal neurons in response to cocaine and haloperidol. J Neurosci 28: 5671–5685.
42. Tzschentke TM (1998) Measuring reward with the conditioned place preference paradigm: A comprehensive review of drug effects, recent progress and new issues. Prog Neurobiol 56: 613–672.
43. Hoffman DC (1994) The noncompetitive NMDA antagonist MK-801 fails to block amphetamine-induced place conditioning in rats. Pharmacol Biochem Behav 47: 907–912.
44. Miyamoto Y, Yamada K, Nagai T, Mori H, Mishina M, et al. (2004) Behavioural adaptations to addictive drugs in mice lacking the NMDA receptor epsilon1 subunit. Eur J Neurosci 19: 151–158.
45. Zhang L, Kitaichi K, Fujimoto Y, Nakayama H, Shimizu E, et al. (2006) Protective effects of minocycline on behavioral changes and neurotoxicity in mice after administration of methamphetamine. Prog Neuropsychopharmacol Biol Psychiatry 30: 1381–1393.
46. Hagiwara H, Iyo M, Hashimoto K (2009) Mithramycin protects against dopaminergic neurotoxicity in the mouse brain after administration of methamphetamine. Brain Res 1301: 189–196.
47. Chen H, Wu J, Zhang J, Fujita Y, Ishima T, et al. (2012) Protective effects of the antioxidant sulforaphane on behavioral changes and neurotoxicity in mice after the administration of methamphetamine. Psychopharmacologyin press.
48. Franklin KBL, Paxinos G (1997) The mouse brain in stereotaxic coordinates. San Diego, CA: Academic Press.
49. Fujita Y, Kunitachi S, Iyo M, Hashimoto K (2012) The antibiotic minocycline prevents methamphetamine-induced rewarding effects in mice. Pharmacol Biochem Behav 101: 303–306.
50. Shi X, McGinty JF (2007) Repeated amphetamine treatment increases phosphorylation of extracellular signal-regulated kinase, protein kinase B, and cyclase response element-binding protein in the rat striatum. J Neurochem 103: 706–713.

Astrocyte-induced cortical vasodilation is mediated by D-serine and endothelial nitric oxide synthase

Jillian L. LeMaistre Stobart[a,b,1], Lingling Lu[a,b,1], Hope D. I. Anderson[c,d], Hisashi Mori[e], and Christopher M. Anderson[a,b,2]

[a]Department of Pharmacology and Therapeutics, University of Manitoba, Winnipeg, MB, Canada R3E 0T6; [b]Division of Neurodegenerative Disorders, St. Boniface Hospital Research, Winnipeg, MB, Canada R2H 2A6; [c]Faculty of Pharmacy, University of Manitoba, Winnipeg, MB, Canada R3E 0T5; [d]Canadian Centre for Agri-Food Research in Health and Medicine, St. Boniface Hospital Research, Winnipeg, MB, Canada R2H 2A6; and [e]Department of Molecular Neuroscience, Graduate School of Medicine and Pharmaceutical Sciences, University of Toyama, Toyama 930-0194, Japan

Edited by Solomon H. Snyder, The Johns Hopkins University School of Medicine, Baltimore, MD, and approved January 11, 2013 (received for review September 14, 2012)

Astrocytes play a critical role in neurovascular coupling by providing a physical linkage from synapses to arterioles and releasing vaso-active gliotransmitters. We identified a gliotransmitter pathway by which astrocytes influence arteriole lumen diameter. Astrocytes synthesize and release NMDA receptor coagonist, D-serine, in response to neurotransmitter input. Mouse cortical slice astrocyte activation by metabotropic glutamate receptors or photolysis of caged Ca^{2+} produced dilation of penetrating arterioles in a manner attenuated by scavenging D-serine with D-amino acid oxidase, deleting the enzyme responsible for D-serine synthesis (serine racemase) or blocking NMDA receptor glycine coagonist sites with 5,7-dichlorokynurenic acid. We also found that dilatory responses were dramatically reduced by inhibition or elimination of endothelial nitric oxide synthase and that the vasodilatory effect of endothelial nitric oxide synthase is likely mediated by suppressing levels of the vasoconstrictor arachidonic acid metabolite, 20-hydroxy arachidonic acid. Our results provide evidence that D-serine coactivation of NMDA receptors and endothelial nitric oxide synthase is involved in astrocyte-mediated neurovascular coupling.

two-photon | functional hyperemia | Ca^{2+} uncaging

Cerebral blood flow is regulated by autoregulation, which maintains constant flow during changes in systemic blood pressure, and functional hyperemia, which refers to matched increases in blood flow to brain areas with high neuronal energy demand. Intracerebral arterioles and capillaries account for 30–40% of total cerebrovascular blood flow resistance (1), and therefore, changes to the diameter of small penetrating cortical vessels result in significant changes in local cerebral blood flow. Astrocytes have endfeet directly apposed to these resistance vessels and are critical regulators of arteriole lumen diameter. Astrocyte endfeet express Ca^{2+}-activated K^+ channels that gate vasodilatory K^+ efflux in response to glutamatergic input (2, 3). Glutamate neurotransmission also causes Ca^{2+}-dependent arachidonic acid (AA) metabolism and release of vasodilatory AA metabolites from astrocytes, including prostaglandin E_2 (PGE_2), produced by cyclooxygenase (COX), and epoxyeicosatrienoic acids (EETs), produced by cytochrome P450 epoxygenase (4–8). Astrocyte-derived AA can also be metabolized by cytochrome P450 ω-hydroxylase to the vasoconstrictor, 20-hydroxyeicosatetranoic acid (20-HETE) (4, 6–8). Ambient tissue oxygen levels dictate whether astrocytes produce AA-dependent vasodilation or vasoconstriction in brain slices and isolated retina (6, 7). Production of 20-HETE is preferred at high pO_2 (95% O_2 in solution) (6–8), whereas pO_2 closer to physiologic levels (20% O_2) inhibits prostaglandin-lactate transporter activity, producing high extracellular PGE_2 levels (7) and reduced 20-HETE synthesis (6).

Application of glutamate or NMDA directly to the brain surface dilates pial arteries (9, 10) by a mechanism mediated by NMDA receptors (9–12) and neuronal nitric oxide synthase (nNOS) (13–15). Although NO is capable of increasing lumen diameter by directly affecting smooth muscle, it may also trigger vasodilation at physiologic pO_2 by reducing ω-hydroxylase activity and 20-HETE production, thereby shifting the balance of constrictor and dilator AA metabolites derived from astrocytes (4, 16, 17). In vivo, it was suggested NO derived from nNOS, specifically, reduces 20-HETE levels (17), but there is no further evidence of a specific link between nNOS and astrocyte AA metabolism in neurovascular coupling. Endothelial NOS (eNOS) plays a role in baseline brain vascular tone and pathological hyperemia (13, 18–21), but there has not yet been a connection made between eNOS, astrocyte function, and hyperemic vasodilation.

NMDA receptors are activated by binding of glutamate and a coagonist that binds to a strychnine-insensitive glycine regulatory site (22). D-Serine is more effective than glycine as an NMDA receptor coagonist (23–25) and has a brain distribution that closely parallels that of NMDA receptors (26). In addition, D-serine is extensively distributed in glial cells (26, 27), is released as a gliotransmitter by Ca^{2+}-dependent exocytosis in response to glutamatergic input (28), and contributes to astrocyte–neuron communication (29–31). Given the established role of NMDA receptors in hyperemic blood flow regulation, we hypothesized that astrocyte D-serine is directly involved in regulating the lumen diameter of brain resistance vessels. We showed previously that isolated middle cerebral arteries dilated in response to exogenous glutamate and D-serine treatment by an NMDA receptor-mediated mechanism (32). The goal of the current study was to determine whether endogenous D-serine is involved in astrocyte-mediated neurovascular coupling in cortical penetrating arterioles. We demonstrated that endogenous D-serine contributes to the vasodilatory response produced by direct astrocyte activation. We also provide evidence that NMDA receptors and eNOS are involved in this response, identifying a signal linking astrocytes and eNOS-mediated vasodilation.

Results

Metabotropic Glutamate Receptor Activation Causes D-Serine–Mediated Dilation of Cortical Arterioles. Immunohistochemistry in fixed cortical slices revealed D-serine immunoreactivity in astrocyte endfeet apposed to penetrating arterioles (Fig. 1). D-Serine signal (Fig. 1*A*) was detected in cells coexpressing the astrocyte marker, GFAP (Fig. 1*B*), around arterioles labeled with isolectin B_4 (Fig. 1*C*). This suggests there is a D-serine pool in close proximity to cortical supply vessels. Separately, the metabotropic glutamate receptor (mGluR) agonist, (±)-1-aminocyclopentane-*trans*-

Author contributions: H.D.I.A. and C.M.A. designed research; J.L.S. and L.L. performed research; H.M. contributed new reagents/analytic tools; J.L.S., L.L., H.D.I.A., and C.M.A. analyzed data; and J.L.S. and L.L. wrote the paper.

The authors declare no conflict of interest.

This article is a PNAS Direct Submission.

[1]J.L.S. and L.L. contributed equally to this work.

[2]To whom correspondence should be addressed. E-mail: chris.anderson@med.umanitoba.ca.

This article contains supporting information online at www.pnas.org/lookup/suppl/doi:10.1073/pnas.1215929110/-/DCSupplemental.

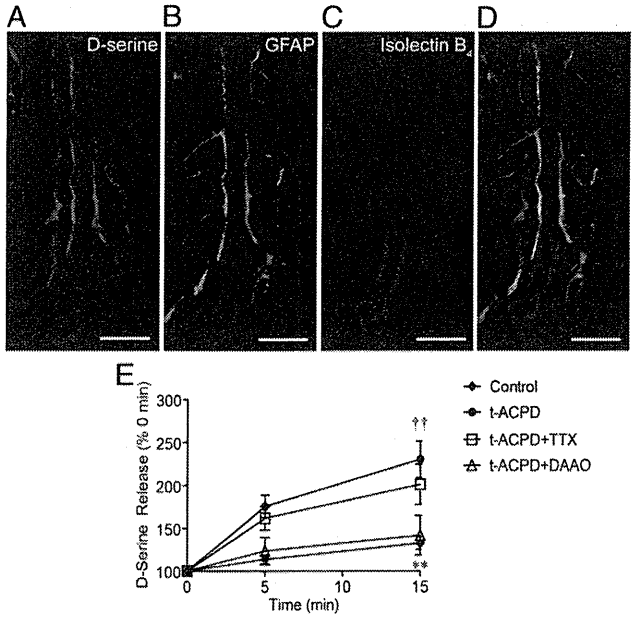

Fig. 1. D-serine localization to perivascular astrocyte endfeet in fixed cortical slices. (*A–D*) D-serine immunoreactivity (*A*, red) was localized to perivascular sites colabeled with the astrocyte marker, GFAP (*B*, green) in glutaraldehyde-fixed cortical slices (30 μm) from 14–19-d-old mice. Cerebrovasculature was labeled with isolectin B_4 (*C*, blue). (*D*), Overlay of *A–C* (scale bar, 20 μm). (*E*) mGluR agonist *t*ACPD (100 μM) induced significant release of D-serine from brain slices compared with untreated controls. Detection was eliminated by coexposure to DAAO (0.1 Units/mL). Data are mean ± SEM; $^{**}P < 0.0.01$ for *t*ACPD compared with control; †† $P < 0.01$ for *t*ACPD/TTX compared with control using two-way ANOVA with Bonferroni post hoc test.

1,3-dicarboxylic acid (*t*ACPD), has been shown to increase intracellular astrocyte Ca^{2+} levels and dilate local arterioles (7, 33), as well as stimulate D-serine release in a Ca^{2+} and SNARE-protein–dependent manner (28, 34). We confirmed that *t*ACPD treatment of acute cortical slices (100 μM) stimulated significant accumulation of extracellular D-serine after 15 min of exposure using a bulk chemiluminescence assay (Fig. 1*E*). Pretreatment with the D-serine catabolic enzyme, D-amino acid oxidase (DAAO), significantly reduced extracellular D-serine accumulation, indicating specific detection of D-serine. Tetrodotoxin (TTX) pretreatment had no effect, suggesting neuronal D-serine pools accessible by depolarization (35) are not involved in this response.

We exposed cortical slices to *t*ACPD and simultaneously monitored perivascular astrocyte Ca^{2+} and neighboring arteriole diameter in real time using two-photon laser scanning microscopy (Fig. 2 *A–C*). In slices maintained in artificial cerebrospinal fluid (aCSF) with 20% O_2, *t*ACPD enhanced rhodamine-2 fluorescence in astrocytes in a manner temporally associated with dilatory responses in cortical arterioles (Fig. 2*D*). *t*ACPD produced a maximal lumen diameter increase of 3.7 ± 0.1%, 75 s after exposure (Fig. 2*E*; maximal of 4.1 ± 0.8% without fixing the time point). Dilatory responses were assessed as area under the curve (AUC) between time 0 (*t*ACPD addition) and return to baseline (Fig. 2*E*). Preincubation of slices with DAAO (0.1 units/mL) significantly reduced vasodilation (Fig. 2*F*), whereas addition of exogenous D-serine to compete for DAAO activity restored vasodilatory responses. *t*ACPD-induced vasodilation in cortical slices isolated from mice lacking the D-serine synthesis enzyme, serine racemase (SR) was dramatically reduced, further indicating an important role for D-serine (Fig. 2*G*). These experiments demonstrate that perivascular astrocytes contain D-serine that can be released in quantities sufficient to increase arteriolar lumen diameter in glutamatergic neurotransmission simulated by mGluR activation. TTX pretreatment did not affect vasodilatory responses (Fig. 2*H*), arguing against an effect of D-serine derived from neuronal stores accessed by depolarization.

Direct Astrocyte Activation Causes D-Serine–Dependent Dilation of Cortical Arterioles. To directly link astrocyte Ca^{2+} elevations with vasodilatory responses, we stimulated increases in cytoplasmic Ca^{2+} levels of single rhodamine-2-labeled perivascular astrocytes using flash photolysis of the caged Ca^{2+} compound, o-nitrophenyl-EGTA AM (NP-EGTA; Fig. S1). Astrocyte Ca^{2+} (rhodamine-2) and arteriole diameter were subsequently monitored (Fig. 3 *A–C*). Astrocyte Ca^{2+} increases consistently correlated with dilation of neighboring cortical arterioles (Fig. 3*D*, representative experiment). Average vasodilation peaked at 5.7 ± 0.2%, 105 s after stimulation (Fig. 3*B*; 7.0 ± 0.9% without fixing the time point). DAAO significantly reduced vasodilation in a manner reversed by addition of exogenous D-serine after flash photolysis (Fig. 3*F*). Similarly, vasodilation was significantly inhibited by deletion of SR (Fig. 3*G*). These data demonstrate that endogenous D-serine plays a role in cortical vasodilation resulting from direct activation of a single perivascular astrocyte by Ca^{2+} uncaging. TTX (1 μM) did not significantly alter

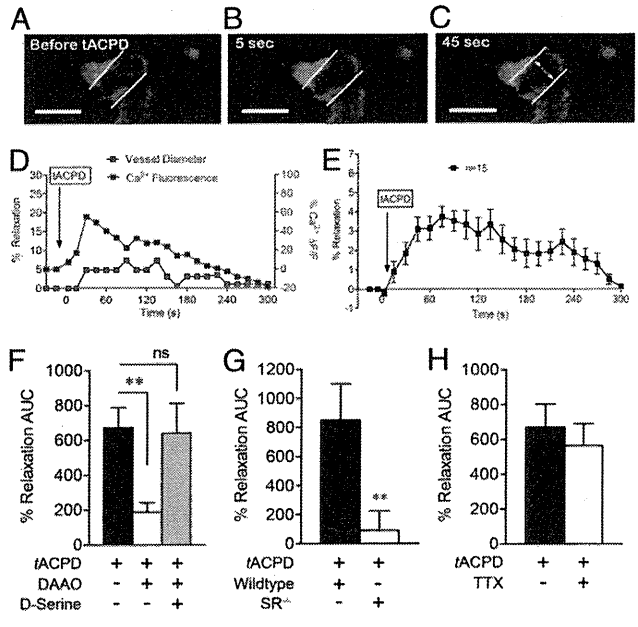

Fig. 2. *t*ACPD induces D-serine–dependent cortical vasodilation. Bath application of *t*ACPD (100 μM) elevated astrocyte Ca^{2+} (green, Rhod 2) and triggered arteriolar (red, isolectin B_4) vasodilation in a temporally correlated manner. (*A–C*) Representative images for a single astrocyte–arteriole pair before *t*ACPD addition (*A*) and 5 (*B*) and 45 (*C*) s after (scale bar, 15 μm). (*D*) Representative plot of changes in astrocyte Ca^{2+} (blue) and arteriole diameter (red) after *t*ACPD treatment. (*E*) Plot of average dilation of 15 vessels after *t*ACPD treatment over 300 s. Data are mean ± SEM. (*F*), DAAO significantly inhibited vasodilation of arterioles after *t*ACPD application, whereas exogenous D-serine (100 μM) with DAAO recovered the dilatory effect of *t*ACPD. (*G*) Genetic deletion of SR ($SR^{-/-}$) eliminated the vasodilatory response to *t*ACPD. (*H*) TTX did not affect *t*ACPD-induced vasodilation. For *G* and *H*, data are mean ± SEM of total AUC for individual plots of percent relaxation versus time. $^{**}P < 0.01$ using one-way ANOVA with Student Newman–Keuls test (>2 groups) or *t* tests (2 groups).

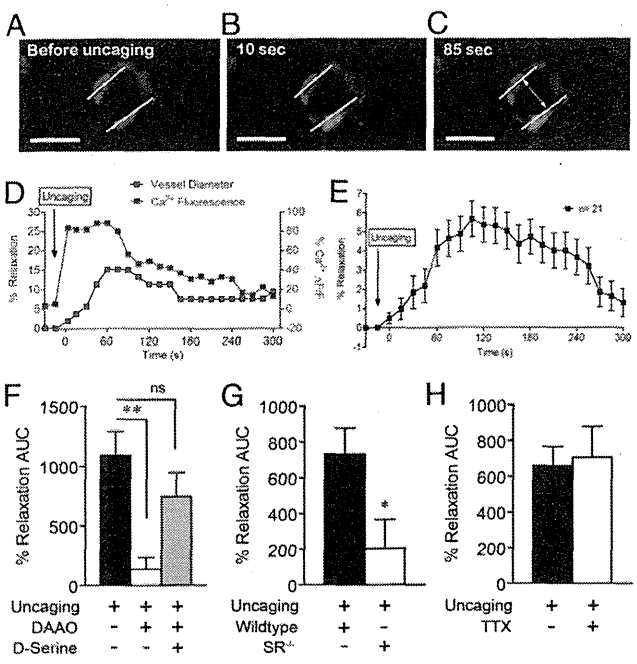

Fig. 3. Direct astrocyte Ca^{2+} uncaging leads to D-serine–dependent cortical vasodilation. Flash photolysis of o-nitrophenyl-EGTA in perivascular astrocyte endfeet stimulated elevation of local Ca^{2+} levels (green, Rhod 2) in a manner that temporally corresponded with an increase in lumen diameter of a neighboring arteriole (red, isolectin B_4). (*A–C*) Representative images of a single perivascular astrocyte and arteriole are shown before (*A*) and after (*B* and *C*) flash photolysis (scale bar, 15 μm). (*D*) Representative plot of changes in astrocyte Ca^{2+} (blue) and arteriole diameter (red) after photolysis. (*E*) Plot of average dilation of 21 vessels after astrocyte Ca^{2+} uncaging over 300 s. Data are mean ± SEM. (*F*) DAAO (0.1 Units/mL) significantly inhibited vasodilation induced by direct astrocyte activation, whereas exogenous D-serine (100 μM) with DAAO recovered the dilatory effect. (*G*) Genetic deletion of SR ($SR^{-/-}$) eliminated the vasodilatory response to astrocyte Ca^{2+} uncaging. (*H*) TTX (1 μM) did not affect vasodilation induced by astrocyte Ca^{2+} uncaging. For *G* and *H*, data are mean ± SEM of total AUC for individual plots of percent relaxation versus time. $*P < 0.05$, $**P < 0.01$ using one-way ANOVA with Student Newman–Keuls test (>2 groups) or *t* tests (2 groups).

vasodilatory responses (Fig. 3*H*), suggesting neuronal excitation is not necessary for direct astrocyte-mediated vasodilation.

D-Serine–Dependent Vasodilation Is Dependent on Glutamate Corelease and NMDA Receptors. Cortical slices were exposed to the NMDA receptor competitive glycine/D-serine coagonist site antagonist 5,7-dichlorokynurenic acid (DCKA; 100 μM) or the competitive glutamate-site antagonist 2-amino-5-phosphonopentanoate (AP5; 50 μM), before flash photolysis of caged Ca^{2+}. Both DCKA and AP5 significantly reduced vasodilatory responses (Fig. 4*A*). Preincubation of cortical slices with glutamate dehydrogenase (GDH; 1 U/mL) also attenuated arteriole dilation resulting from flash photolysis (Fig. 4*B*), indicating that both glutamate and D-serine (Figs. 2 and 3) are involved in astrocyte-mediated vasodilation. In agreement, *t*ACPD caused TTX-independent bulk release of endogenous glutamate from cortical slices (Fig. 4*C*), supporting the idea that glutamate and D-serine are coreleased from astrocytes and play a joint role in neurovascular coupling.

Astrocyte-Mediated Vasodilation Is Dependent on PGE_2 and eNOS. Our data demonstrate that intact endothelium and eNOS are required for D-serine and glutamate to increase lumen diameter in isolated middle cerebral arteries (32). We thus tested the hypothesis that D-serine and glutamate-induced vasodilation in cortical slice arterioles is mediated by eNOS. In response to astrocyte Ca^{2+} uncaging, genetic deletion of eNOS dramatically attenuated increases in lumen diameter compared with treatment controls (Fig. 5*A*). We also measured vasodilatory responses to an exogenous glutamate and D-serine mixture (10 μM each with 1 μM TTX) in the presence and absence of the eNOS inhibitor, N5-(1-iminoethyl)-L-ornithine (L-NIO; 3 μM). L-NIO significantly reduced arteriole dilation by glutamate and D-serine (Fig. 5*B*), directly linking D-serine with eNOS activity and vasodilation in cortical slices.

Several studies have demonstrated that astrocyte-induced cortical vasodilation is mediated by COX-dependent metabolism of AA to PGE_2 (5, 7, 33). We therefore tested for PGE_2 involvement in our model by using indomethacin (INM; 100 μM) to inhibit COX. INM alone reduced vasodilation produced by astrocyte Ca^{2+} uncaging by 87% (Fig. 5*C*). This is not significantly different from the L-NIO-mediated reduction (55%). Combined, INM and L-NIO significantly enhanced the effect of L-NIO alone, producing vasoconstriction in response to astrocyte Ca^{2+} uncaging (Fig. 5*C*). *t*ACPD-induced astrocyte activation increased PGE_2 levels in a manner independent of L-NIO or genetic eNOS elimination (Fig. 5*D*), indicating that eNOS does not cause vasodilation by directly influencing PGE_2.

eNOS Causes Vasodilation by Suppressing 20-HETE Production. There is substantial evidence that NO inhibits production of the vasoconstrictor AA metabolite 20-HETE (36), leading to vasodilation in brain microvasculature (4, 17), but any contribution of eNOS to this pathway is yet to be identified. In our hands, brain slice production of 20-HETE in the presence of *t*ACPD was significantly enhanced in eNOS-null cortical slices (Fig. 6*A*), demonstrating that eNOS activity suppresses 20-HETE production in this model. To determine whether suppression of 20-HETE participates in eNOS-mediated vasodilation, we examined the effect of eNOS inhibition by L-NIO in the absence of a functional 20-HETE production pathway, suppressed by the

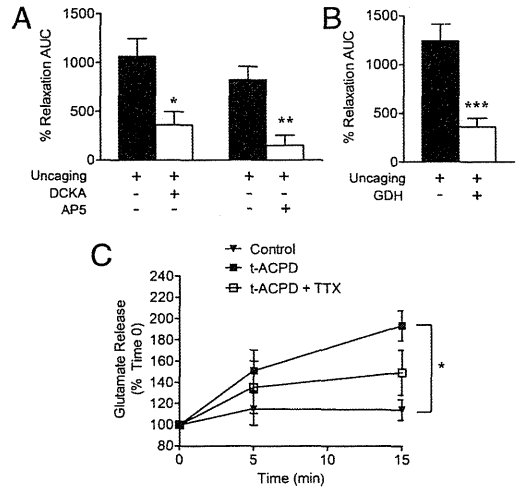

Fig. 4. Cortical vasodilation by D-serine is dependent on glutamate and NMDA receptors. (*A*) *t*ACPD induced significant TTX-insensitive (1 μM) glutamate release, relative to control cortical slices ($*P < 0.05$ using two-way ANOVA with Bonferroni test). (*B*) GDH (1 U/mL) significantly reduced arteriole vasodilation induced by astrocyte Ca^{2+} uncaging ($***P < 0.001$, *t* test). (*C*) Competitive NMDA receptor antagonists DCKA (glycine site, 100 μM) and AP5 (glutamate site, 50 μM) significantly blocked arteriole vasodilation induced by direct astrocyte Ca^{2+} uncaging ($*P < 0.05$; $**P < 0.01$, one-way ANOVA with Student Newman–Keuls test). All data are mean ± SEM.

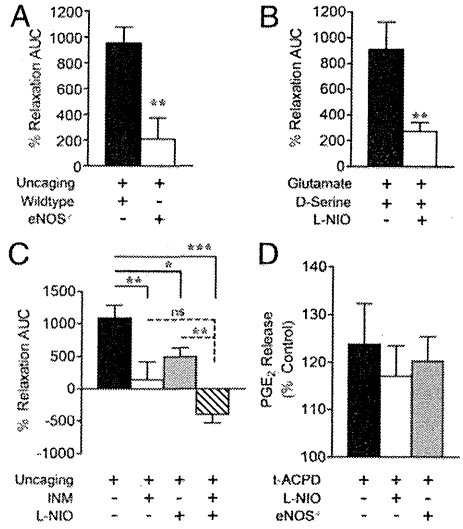

Fig. 5. Astrocyte-induced cortical vasodilation is mediated by PGE_2 and eNOS. (*A*) eNOS-null mice displayed reduced cortical vasodilatory efficacy in response to astrocyte Ca^{2+} uncaging compared with C57 wild-type mice (**$P < 0.01$, *t* test). (*B*) Coapplication of glutamate (10 μM), D-serine (10 μM), and TTX (1 μM) produced cortical slice vasodilation sensitive to inhibition by the eNOS selective antagonist L-NIO (3 μM, **$P < 0.01$, *t* test). (*C*) Both the COX inhibitor INM (100 μM) and eNOS inhibitor L-NIO (3 μM) significantly reduced vasodilation in response to astrocyte Ca^{2+} uncaging. Combined INM and L-NIO caused significant vasoconstriction in response to astrocyte Ca^{2+} uncaging (*$P < 0.05$, **$P < 0.01$, ***$P < 0.001$ using one-way ANOVA with Student Newman–Keuls test). (*D*) PGE_2 release from cortical slices was measured by ELISA 5 min after *t*ACPD treatment and was not significantly affected by treatment with L-NIO (3 μM) or genetic eNOS deletion (ns, $P > 0.05$ using one-way ANOVA with Student Newman–Keuls test). All data are mean ± SEM.

CYP4A (ω-hydroxylase) inhibitor *N*-hydroxy-N'-(4-n-butyl-2-methylphenyl)formamidine (HET0016; 100 nM). Vasodilation induced by astrocyte Ca^{2+} uncaging was significantly inhibited by L-NIO alone but not in combination with HET0016 (Fig. 6*B*), suggesting that eNOS vasodilation is dependent on activity of the 20-HETE pathway.

Discussion

Here, we provided evidence that endogenous D-serine is a mediator of neurovascular coupling. D-Serine was responsible for astrocyte-induced dilation of penetrating cortical arterioles in a manner dependent on coavailability of extracellular glutamate and NMDA receptors. We also demonstrated that astrocyte-mediated cortical vasodilation is at least partially dependent on eNOS-derived suppression of 20-HETE.

Several lines of evidence support involvement of astrocyte D-serine in dilation of penetrating cortical arterioles in brain slices. D-Serine immunoreactivity was identified in perivascular astrocyte endfeet, in agreement with a previous report (26). Also consistent with published data (28), we found that simulating glutamatergic neurotransmission by exposing cortical slices to *t*ACPD caused significant efflux of D-serine into the bathing medium (28). These data together suggest there is a source of D-serine available for regulated release at the neurovascular unit. We then showed that DAAO and SR deletion significantly inhibited dilation of brain slice–penetrating cortical arterioles induced by *t*ACPD. This observation established a critical role for endogenous D-serine in regulating brain vascular lumen diameter, and this role is supported further by the demonstration that vasodilatory effects were mitigated by interfering with specific binding for D-serine in the NMDA receptor complex by DCKA. Because *t*ACPD activates both neuronal and astrocytic mGluRs, we considered the possibility that the vasodilatory effect of D-serine is independent of astrocyte activation by *t*ACPD. Although the failure of TTX to suppress D-serine release and cortical vasodilation argues against this idea, we more precisely ascertained the role of astrocytes in D-serine–mediated vasodilation by using flash photolysis of caged Ca^{2+} (NP-EGTA) in perivascular astrocyte endfeet. Direct astrocyte activation was sufficient to increase arteriolar lumen diameter in cortical slices. Moreover, uncaging-induced vasodilation was blocked by more than 88% by DAAO and 72% by SR deletion, providing further support for a vasodilatory pathway originating with glutamate neurotransmission and leading to astrocyte Ca^{2+} elevation, D-serine release from astrocytes, and vascular smooth muscle relaxation.

The impact of observed changes to the lumen diameter on blood flow is an important consideration. Poiseuille's Law dictates that resistance to blood flow decreases as a function of the fourth power of any increases in lumen diameter. Therefore, a 7% increase in lumen diameter (average achievement with uncaging) reduces resistance by a more impressive magnitude of 24%. In addition, comparisons across experimental conditions are critical because some models use preconstriction paradigms to achieve a much higher magnitude of vasodilation (33, 37). Our observations are consistent with vasodilation magnitudes observed by another group using brain slices maintained without preconstriction at equal aCSF oxygenation (7). These points, coupled with observations that vasodilation in vitro likely underestimates COX-mediated vasodilation seen in pressurized vessels in vivo (5), support speculation that our observed vasodilatory magnitudes in vitro translate into meaningful blood flow changes in vivo.

Our data support a vasodilatory mechanism of D-serine mediated by coactivation of NMDA receptors with glutamate. Again, cortical vasodilation induced by astrocyte Ca^{2+} uncaging was significantly attenuated by DCKA, directly indicating that activation of NMDA receptor glycine sites is involved. Importantly, this effect was also inhibited by AP5, indicating that occupation of the NMDA receptor glutamate binding site is also required for vasodilation in this paradigm. Paired involvement of glutamate and D-serine is further supported by our observations that *t*ACPD stimulated both glutamate and D-serine release (Figs. 4*C* and 1*E*, respectively) and that the presence of the glutamate catabolic enzyme GDH eliminated cortical vasodilation initiated by Ca^{2+} uncaging. Overall, these results show that both coagonists of NMDA receptors are required for a significant component of astrocyte-induced vasodilation in cortical slices. There is a report that AP5 does not affect cortical vasodilation in response to *t*ACPD (33). Although this is seemingly

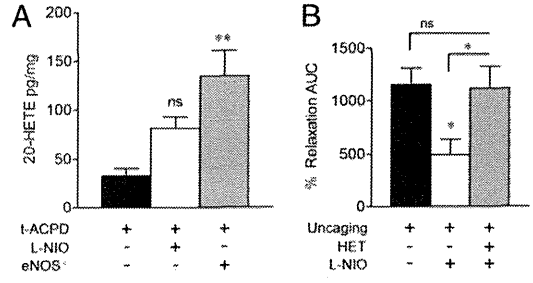

Fig. 6. eNOS inhibits 20-HETE production. (*A*) Cortical slice 20-HETE production in response to *t*ACPD was statistically unchanged by L-NIO (ns, $P > 0.05$) and increased by eNOS deletion (**$P < 0.01$, one-way ANOVA with Student Newman–Keuls test). (*B*) Alone, L-NIO (3 μM) significantly reduced cortical vasodilation induced by astrocyte Ca^{2+} uncaging (*$P < 0.05$, one-way ANOVA with Student Newman–Keuls test). This effect was lost in the presence of HET0016 (HET, 100 nM; ns, $P > 0.05$), which interferes with 20-HETE formation. All data are mean ± SEM.

inconsistent with our results, Zonta et al. (33) used artificial CSF equilibrated with 95% O_2, which is a condition that is dramatically different from ours (20%) and favors production of the smooth muscle constrictor 20-HETE (4, 6, 7). This may mask the vasodilatory effects of D-serine and NMDA receptors, making the models difficult to compare appropriately. The cellular source of NMDA receptors responsible for vasodilation in our model is not clear. Our previous work indicates that brain arterial endothelial cells express NMDA receptors capable of initiating a vasodilatory response to extraluminally applied glutamate and D-serine (32). Current data indicate that eNOS contributes to astrocyte-mediated vasodilation and that TTX-sensitive neuronal Na^+ channels, and therefore direct vessel innervation (38), are not required for vasodilation downstream of astrocyte activation. All of these observations tempt speculation that endothelial, rather than neuronal, NMDA receptors participate in astrocyte-mediated vasodilation, but definitive experiments have yet to be performed.

A clear conclusion drawn from our current findings is that eNOS participates in astrocyte-mediated dilation of penetrating cortical arterioles. NO is central to NMDA receptor-mediated neurovascular coupling (10, 39, 40), but only a role for nNOS, specifically, has been described (14, 39, 41). Our finding that a mixture of glutamate or NMDA and D-serine can dilate isolated cerebral arteries by an endothelium and eNOS-dependent mechanism (32) gave rise to the hypothesis that eNOS may be involved in vasodilation initiated by astrocyte gliotransmission in situ. In support of this hypothesis, cortical vasodilation induced by astrocyte Ca^{2+} uncaging was significantly inhibited by L-NIO at a concentration (3 μM) yielding strong selectivity for eNOS (42, 43) and by genetic eNOS deletion. D-serine was also linked directly to eNOS activity in cortical slice arterioles, as L-NIO inhibited vasodilation induced by exogenous application of glutamate/D-serine (10 μM each) in the presence of TTX. In functional hyperemia in vivo, a recent cat study concluded that both nNOS and eNOS participate in vasodilatory responses, with eNOS becoming more prominent at lower levels of neuronal activity and nNOS dominating at higher neuronal activation levels (44). We did not compare the relative roles of eNOS and nNOS in cortical vasodilation induced by *t*ACPD or direct astrocyte activation. Further studies targeting eNOS and nNOS loss of function will assist in determining the relative roles of these isoforms and the cell types in which they are expressed.

Our *t*ACPD and astrocyte Ca^{2+} uncaging paradigms closely resemble those used in several previous studies demonstrating the astrocyte-mediated cortical or hippocampal vasodilation is mediated by the COX metabolite PGE_2 (5–7, 33). Therefore, it is important to address how discovery of a role for eNOS fits with the established COX-mediated mechanism. We found agreement with previous studies (5–7) by showing that COX metabolites also contributed to astrocyte-mediated vasodilation, as INM inhibited vascular responses to Ca^{2+} uncaging. Addition of INM to L-NIO treatment resulted in a loss of vasodilatory effect greater than that achieved with L-NIO alone and actually produced smooth muscle constriction, suggesting that eNOS and COX pathways are additive. Additivity is further supported by the observation that astrocyte-activated eNOS has no direct effect on PGE_2 levels (Fig. 5*C*). It has been reported that NO modulates the vascular effects of AA metabolites by inhibiting cytochrome P450 enzymes that produce 20-HETE and EETs (4). In our hands, cortical 20-HETE content in response to *t*ACPD treatment was significantly enhanced in $eNOS^{-/-}$ slices. This demonstrates that eNOS-derived NO inhibits 20-HETE production and suggests that vasodilation may result from NO-induced suppression of the 20-HETE influence on smooth muscle tone. Support for functional suppression of the vascular effects of 20-HETE comes from experiments using L-NIO and an inhibitor of CYP4A ω-hydroxylase (HET0016), which is the enzyme responsible for 20-HETE formation. The ability of L-NIO to attenuate vasodilatory responses to astrocyte Ca^{2+} uncaging was lost in the presence of HET0016, suggesting that the vasodilatory role of eNOS-derived NO depends on an active 20-HETE production pathway. Overall, our data support dual astrocyte-mediated vasodilatory mechanisms working together. We and others demonstrated that astrocyte activation leads to direct COX-dependent, PGE_2-mediated increases in cortical arteriole lumen diameter. Our data support the idea that astrocyte activation also leads to eNOS activity and suppression of 20-HETE levels, thus facilitating the direct PGE_2-mediated vasodilation.

Materials and Methods

Chemicals and Animals. All chemicals were purchased from Sigma-Aldrich, unless otherwise noted. Animal procedures were approved by the Office of Research Ethics and Compliance Animal Care Committee for the Bannatyne Campus, University of Manitoba. SR deletion mice were generated from C57BL/6-derived embryonic stem cells transfected with the gene-targeting vector containing C57BL/6 mouse genomic DNA and were expanded by crossing with C57BL/6 mice (45). Wild-type littermate controls were used for experiments comparing control to SR knockout phenotypes. eNOS deletion mice were purchased from Jackson Laboratories and bred at the R.O. Burrell Lab at St. Boniface Hospital Research. C57BL/6 was used as the control strain.

Brain Slice Preparation and Two-Photon Laser Scanning Microscopy. Brains from CD1 or C57BL/6 mice (14–19 d old) were placed in ice-cold cutting buffer (2.5 mM KCl, 1.25 mM NaH_2PO_4, 10 mM $MgSO_4$, 5 mM $CaCl_2$, 26 mM $NaHCO_3$, 10 mM glucose, 230 mM sucrose) bubbled with 95% O_2 and 5% CO_2. Slices were cut on a vibrating blade microtome (350 μm) and were then maintained in aCSF (126 mM NaCl, 2.5 mM KCl, 1.25 mM NaH_2PO_4, 2 mM $MgCl_2$, 2 mM $CaCl_2$, 26 mM $NaHCO_3$, 10 mM glucose) equilibrated with 95% O_2, 5% CO_2, and heated to 35 °C. After 1 h, slices were loaded with the Ca^{2+} indicator dye, Rhodamine-2 AM (10 μM; Invitrogen), and *Griffonia simplicifolia* 1 Isolectin B_4 tagged with Alexa Fluor 488 (5 μg/mL; Invitrogen). Two-photon imaging proceeded on the stage of an upright microscope in aCSF equilibrated with 20% O_2, 5% CO_2, and 75% N_2. Scans were performed using an excitation wavelength of 800 nm, delivered through an Ultima multiphoton scanhead, with dual galvanometers for imaging and uncaging (Prairie Technologies), by a pulsed Ti-sapphire laser (Coherent Inc.). For astrocyte Ca^{2+} uncaging, cortical slices were incubated with o-nitrophenyl-EGTA AM (10 μM; Invitrogen) for 1 h. Cytoplasmic photoliberation of Ca^{2+} was achieved using functional mapping software (TriggerSync, Prairie Technologies) to guide a 700 nm/100 ms laser pulse through a voltage-controlled pockels cell. Images were analyzed every 15 s using PrairieView software to determine vessel lumen diameter, as marked by isolectin staining. Changes in vessel lumen diameter were correlated with astrocyte rhodamine-2 Ca^{2+} fluorescence intensity changes, which were measured using ImageJ.

D-Serine and Glutamate Release Assays. Acute brain slices were incubated in aCSF equilibrated with 20% O_2/5% CO_2 and then stimulated with *t*ACPD (100 μM) for 15 min. Some slices were pretreated with DAAO (0.1 U/mL) or TTX (1 μM) for 20 min. During *t*ACPD stimulation, samples of aCSF were collected at 0 min, 5 min, or 15 min for measurement of D-serine and glutamate concentrations. D-serine release was measured by chemiluminescent assay, as described previously with minor modification (46, 47). We mixed 10 μl of each sample with 100 μl of aCSF containing 100 mM Tris·HCl, pH 8.8, 20 U/mL peroxidase, and 8 μl of luminol. Samples were incubated 15 min to decrease background signal of luminol, and then 10 μl of DAAO (75 U/mL) was added, where applicable. Chemiluminescence kinetics was recorded for 5 min at room temperature using a TD-20/20 Luminometer (Turner Designs). D-serine concentrations were calculated based on a standard curve. Glutamate release was determined at each time point by using Amplex Red Glutamic Acid/Glutamate Oxidase Assay Kit (Invitrogen).

PGE_2 and 20-HETE ELISAs. Acute brain slices were incubated in aCSF equilibrated with 20% O_2/5% CO_2 and stimulated with *t*ACPD (100 μM) for 5 min. Some slices were pretreated with TTX (1 μM) with or without L-NIO (3 μM) for 20 min. PGE_2 release in aCSF was measured using the PGE_2 enzyme immunoassay (EIA) Kit (Cayman). For 20-HETE, brain slices were lysed and 20-HETE production was measured by 20-HETE ELISA Kit (Detroit R&D, Inc.).

D-Serine Immunohistochemistry. D-serine immunostaining was modified from the procedure by Schell et al. (1995) (26). Brains from 14–19-d-old CD1 mice were fixed (5% glutaraldehyde, 0.5% PFA, 0.2% $Na_2S_2O_5$, 0.1 M Na_2PO_4 buffer at pH 7.4) for 24 h and cryopreserved in 30% sucrose. Tissue was then snap-frozen in liquid nitrogen cooled n-hexane and cut into 30 μm sections. Slices were reduced for 20 min at room temperature in 0.2% $Na_2S_2O_5$ and 0.5% $NaBH_4$ in 0.1 M Tris-buffered saline (TBS; pH 7.4) and rinsed with 0.2% $Na_2S_2O_5$ in TBS for 45 min. Tissue was blocked in 4% goat serum, 0.2% Triton X-100, and 0.2% $Na_2S_2O_5$ in 0.1 M TBS for 2 h and then incubated in 0.1 M TBS (pH 7.2) with 2% goat serum, 0.1% Triton X-100, and primary antibodies: rabbit anti-D-serine (Millipore), mouse anti-GFAP, and *G. simplicifolia* 1 Isolectin B_4 tagged with Alexa Fluor 488 (Invitrogen) for 48 h. Secondary antibodies Alexa Fluor 633 goat anti-rabbit IgG (H+L) (Invitrogen) and Alexa Fluor 568 goat anti-mouse IgG (H+L) (Invitrogen) were used for visualization of D-serine and GFAP. Images were collected with a Zeiss LSM510 laser-scanning microscope.

Data Analysis. AUC was calculated from percent vessel relaxation versus time plots. AUC among experimental groups were compared using *t* test for two groups or one-way ANOVA with Student Newman–Keuls post hoc test for three or more groups. The time course of glutamate and D-serine release from slices was analyzed by two-way ANOVA with Bonferroni post hoc tests.

ACKNOWLEDGMENTS. The authors thank Ms. Ayumi Tanaka for SR deletion mouse preparation. Research was supported by an operating grant from the Canadian Institutes of Health Research. J.L.S. was supported by a student award from the Canadian Institutes of Health Research.

1. Iadecola C (2004) Neurovascular regulation in the normal brain and in Alzheimer's disease. *Nat Rev Neurosci* 5(5):347–360.
2. Filosa JA, et al. (2006) Local potassium signaling couples neuronal activity to vasodilation in the brain. *Nat Neurosci* 9(11):1397–1403.
3. Girouard H, et al. (2010) Astrocytic endfoot Ca2+ and BK channels determine both arteriolar dilation and constriction. *Proc Natl Acad Sci USA* 107(8):3811–3816.
4. Metea MR, Newman EA (2006) Glial cells dilate and constrict blood vessels: A mechanism of neurovascular coupling. *J Neurosci* 26(11):2862–2870.
5. Takano T, et al. (2006) Astrocyte-mediated control of cerebral blood flow. *Nat Neurosci* 9(2):260–267.
6. Mishra A, Hamid A, Newman EA (2011) Oxygen modulation of neurovascular coupling in the retina. *Proc Natl Acad Sci USA* 108(43):17827–17831.
7. Gordon GR, Choi HB, Rungta RL, Ellis-Davies GC, MacVicar BA (2008) Brain metabolism dictates the polarity of astrocyte control over arterioles. *Nature* 456(7223):745–749.
8. Mulligan SJ, MacVicar BA (2004) Calcium transients in astrocyte endfeet cause cerebrovascular constrictions. *Nature* 431(7005):195–199.
9. Busija DW, Leffler CW (1989) Dilator effects of amino acid neurotransmitters on piglet pial arterioles. *Am J Physiol* 257(4 Pt 2):H1200–H1203.
10. Faraci FM, Breese KR (1993) Nitric oxide mediates vasodilatation in response to activation of N-methyl-D-aspartate receptors in brain. *Circ Res* 72(2):476–480.
11. Bhardwaj A, et al. (2000) P-450 epoxygenase and NO synthase inhibitors reduce cerebral blood flow response to N-methyl-D-aspartate. *Am J Physiol Heart Circ Physiol* 279(4):H1616–H1624.
12. Simandle SA, et al. (2005) Piglet pial arteries respond to N-methyl-D-aspartate in vivo but not in vitro. *Microvasc Res* 70(1–2):76–83.
13. Iadecola C (1993) Regulation of the cerebral microcirculation during neural activity: Is nitric oxide the missing link? *Trends Neurosci* 16(6):206–214.
14. Fergus A, Lee KS (1997) Regulation of cerebral microvessels by glutamatergic mechanisms. *Brain Res* 754(1–2):35–45.
15. Ma J, Ayata C, Huang PL, Fishman MC, Moskowitz MA (1996) Regional cerebral blood flow response to vibrissal stimulation in mice lacking type I NOS gene expression. *Am J Physiol* 270(3 Pt 2):H1085–H1090.
16. Alonso-Galicia M, Hudetz AG, Shen H, Harder DR, Roman RJ (1999) Contribution of 20-HETE to vasodilator actions of nitric oxide in the cerebral microcirculation. *Stroke* 30(12):2727–2734, discussion 2734.
17. Liu X, et al. (2008) Interaction of nitric oxide, 20-HETE, and EETs during functional hyperemia in whisker barrel cortex. *Am J Physiol Heart Circ Physiol* 295(2):H619–H631.
18. Ma J, et al. (1996) L-NNA-sensitive regional cerebral blood flow augmentation during hypercapnia in type III NOS mutant mice. *Am J Physiol* 271(4 Pt 2):H1717–H1719.
19. Pereira de Vasconcelos A, Riban V, Wasterlain C, Nehlig A (2006) Role of endothelial nitric oxide synthase in cerebral blood flow changes during kainate seizures: A genetic approach using knockout mice. *Neurobiol Dis* 23(1):219–227.
20. Hlatky R, et al. (2003) The role of endothelial nitric oxide synthase in the cerebral hemodynamics after controlled cortical impact injury in mice. *J Neurotrauma* 20(10):995–1006.
21. Endres M, Laufs U, Liao JK, Moskowitz MA (2004) Targeting eNOS for stroke protection. *Trends Neurosci* 27(5):283–289.
22. Dingledine R, Borges K, Bowie D, Traynelis SF (1999) The glutamate receptor ion channels. *Pharmacol Rev* 51(1):7–61.
23. Fadda E, Danysz W, Wroblewski JT, Costa E (1988) Glycine and D-serine increase the affinity of N-methyl-D-aspartate sensitive glutamate binding sites in rat brain synaptic membranes. *Neuropharmacology* 27(11):1183–1185.
24. Matsui T, et al. (1995) Functional comparison of D-serine and glycine in rodents: The effect on cloned NMDA receptors and the extracellular concentration. *J Neurochem* 65(1):454–458.
25. Shleper M, Kartvelishvily E, Wolosker H (2005) D-serine is the dominant endogenous coagonist for NMDA receptor neurotoxicity in organotypic hippocampal slices. *J Neurosci* 25(41):9413–9417.
26. Schell MJ, Molliver ME, Snyder SH (1995) D-serine, an endogenous synaptic modulator: Localization to astrocytes and glutamate-stimulated release. *Proc Natl Acad Sci USA* 92(9):3948–3952.
27. Wolosker H, Blackshaw S, Snyder SH (1999) Serine racemase: A glial enzyme synthesizing D-serine to regulate glutamate-N-methyl-D-aspartate neurotransmission. *Proc Natl Acad Sci USA* 96(23):13409–13414.
28. Mothet JP, et al. (2005) Glutamate receptor activation triggers a calcium-dependent and SNARE protein-dependent release of the gliotransmitter D-serine. *Proc Natl Acad Sci USA* 102(15):5606–5611.
29. Panatier A, et al. (2006) Glia-derived D-serine controls NMDA receptor activity and synaptic memory. *Cell* 125(4):775–784.
30. Henneberger C, Papouin T, Oliet SH, Rusakov DA (2010) Long-term potentiation depends on release of D-serine from astrocytes. *Nature* 463(7278):232–236.
31. Yang Y, et al. (2003) Contribution of astrocytes to hippocampal long-term potentiation through release of D-serine. *Proc Natl Acad Sci USA* 100(25):15194–15199.
32. LeMaistre JL, et al. (2012) Coactivation of NMDA receptors by glutamate and D-serine induces dilation of isolated middle cerebral arteries. *J Cereb Blood Flow Metab* 32(3):537–547.
33. Zonta M, et al. (2003) Neuron-to-astrocyte signaling is central to the dynamic control of brain microcirculation. *Nat Neurosci* 6(1):43–50.
34. Martineau M, Galli T, Baux G, Mothet JP (2008) Confocal imaging and tracking of the exocytotic routes for D-serine-mediated gliotransmission. *Glia* 56(12):1271–1284.
35. Rosenberg D, et al. (2010) Neuronal release of D-serine: A physiological pathway controlling extracellular D-serine concentration. *FASEB J* 24(8):2951–2961.
36. Roman RJ (2002) P-450 metabolites of arachidonic acid in the control of cardiovascular function. *Physiol Rev* 82(1):131–185.
37. Koide M, Bonev AD, Nelson MT, Wellman GC (2012) Inversion of neurovascular coupling by subarachnoid blood depends on large-conductance Ca^{2+}-activated K^+ (BK) channels. *Proc Natl Acad Sci USA* 109(21):E1387–E1395.
38. Tong XK, Hamel E (2000) Basal forebrain nitric oxide synthase (NOS)-containing neurons project to microvessels and NOS neurons in the rat neocortex: Cellular basis for cortical blood flow regulation. *Eur J Neurosci* 12(8):2769–2780.
39. Bari F, Errico RA, Louis TM, Busija DW (1996) Interaction between ATP-sensitive K^+ channels and nitric oxide on pial arterioles in piglets. *J Cereb Blood Flow Metab* 16(6):1158–1164.
40. Meng W, Tobin JR, Busija DW (1995) Glutamate-induced cerebral vasodilation is mediated by nitric oxide through N-methyl-D-aspartate receptors. *Stroke* 26(5):857–862, discussion 863.
41. Faraci FM, Brian JE, Jr. (1995) 7-Nitroindazole inhibits brain nitric oxide synthase and cerebral vasodilatation in response to N-methyl-D-aspartate. *Stroke* 26(11):2172–2175, discussion 2176.
42. Chinellato A, Froldi G, Caparrotta L, Ragazzi E (1998) Pharmacological characterization of endothelial cell nitric oxide synthase inhibitors in isolated rabbit aorta. *Life Sci* 62(6):479–490.
43. Rees DD, Palmer RM, Schulz R, Hodson HF, Moncada S (1990) Characterization of three inhibitors of endothelial nitric oxide synthase in vitro and in vivo. *Br J Pharmacol* 101(3):746–752.
44. de Labra C, et al. (2009) Different sources of nitric oxide mediate neurovascular coupling in the lateral geniculate nucleus of the cat. *Front Syst Neurosci* 3:9.
45. Miya K, et al. (2008) Serine racemase is predominantly localized in neurons in mouse brain. *J Comp Neurol* 510(6):641–654.
46. Wolosker H, et al. (1999) Purification of serine racemase: Biosynthesis of the neuromodulator D-serine. *Proc Natl Acad Sci USA* 96(2):721–725.
47. Zhuang Z, et al. (2010) EphrinBs regulate D-serine synthesis and release in astrocytes. *J Neurosci* 30(47):16015–16024.

Supporting Information

Stobart et al. 10.1073/pnas.1215929110

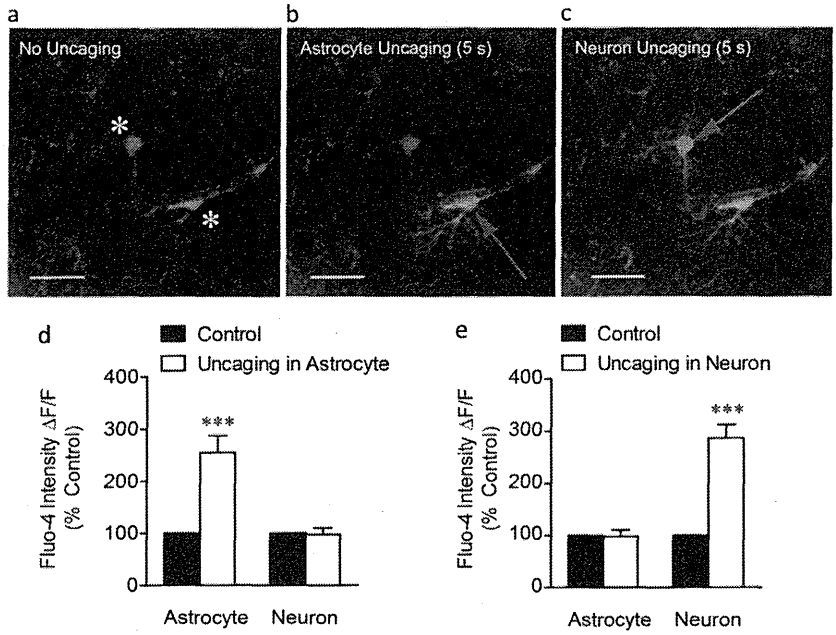

Fig. S1. Flash photolysis is confined to individually targeted astrocytes. Cortical slices were loaded with NP-EGTA (caged Ca^{2+}), Fluo-4 (Ca^{2+} indicator, green channel), and SR-101 (astrocyte-selective dye, red channel). Two-photon flash photolysis (700 nm) was performed in single perivascular astrocytes or neurons using a pulsed infrared laser (Coherent, Inc) and functional mapping software (Prairie Technologies). Ca^{2+} levels were subsequently monitored and analyzed at peak levels (5 s, as shown in Fig. 3). A cortical neurovascular unit is shown before flash photolysis. In *A*, a neuronal cell body with projections toward a cortical arteriole is loaded with Fluo-4 and appears green (white asterisk). A perivascular astrocyte is stained with SR-101 (red) and loaded with Fluo-4 (green) and appears yellow (yellow asterisk). In *B*, the astrocyte is targeted by flash photolysis (red arrow), causing a dramatic enhancement of Fluo-4 fluorescence after 5 s in the astrocyte. In *C*, the neuron is targeted by flash photolysis (red arrow), enhancing Fluo-4 fluorescence after 5 s in the neuronal soma and dendrites. Quantification of these experiments ($n = 3$) showed that astrocyte Ca^{2+} uncaging produced a 2.6-fold increase in astrocyte Ca^{2+} after 5 s with no significant change in neuronal Ca^{2+} levels (*D*). Similarly, neuronal Ca^{2+} uncaging produced a 2.9-fold increase in neuronal Ca^{2+} after 5 s with no significant change in astrocyte Ca^{2+} levels (*E*). All data are mean ± SEM. $^{***}P < 0.001$ compared with control using two-way ANOVA with Bonferroni posttest (scale bar, 50 μm).

Epilepsy & Behavior 24 (2012) 373–376

Contents lists available at SciVerse ScienceDirect

Epilepsy & Behavior

journal homepage: www.elsevier.com/locate/yebeh

Case Report

Acute psychosis during the postictal period in a patient with idiopathic generalized epilepsy: Postictal psychosis or aggravation of schizophrenia? A case report and review of the literature

Eisuke Sakakibara [a,b,*], Takuji Nishida [b,c], Kazuyuki Sugishita [b,d], Seiichiro Jinde [b], Yushi Inoue [c], Kiyoto Kasai [b]

[a] Department of Psychiatry, National Center of Neurology and Psychiatry, National Center Hospital, Japan
[b] Department of Neuropsychiatry, The University of Tokyo Hospital, Japan
[c] National Epilepsy Center, Shizuoka Institute of Epilepsy and Neurological Disorders, Japan
[d] Oji Mental Clinic, Japan

ARTICLE INFO

Article history:
Received 2 April 2012
Revised 10 April 2012
Accepted 21 April 2012
Available online 29 May 2012

Keywords:
Psychotic disorders
Postictal psychosis
Interictal psychosis
Epilepsy
Idiopathic generalized epilepsy
Schizophrenia

ABSTRACT

Postictal psychoses are common comorbid conditions of temporal lobe epilepsy and are reported to be characterized by affective changes. However, postictal psychoses are rare among patients with idiopathic generalized epilepsy, and the causal relationship between postictal psychoses and idiopathic generalized epilepsy is unknown. Here, we report the case of a man who had idiopathic generalized epilepsy and experienced 4 episodes of schizophrenia-like interictal psychosis before the age of 41 years. At the age of 56 years, he experienced a generalized tonic-clonic seizure for the first time in 15 years and developed psychotic symptoms on the next day. Notably, in addition to the schizophrenia-like symptoms, the patient experienced mania-like symptoms such as elated mood, grandiose delusions, agitation, and pressured speech during the last psychotic episode in the postictal period. It was suspected that postictal neuronal processes and a predisposition to endogenous psychosis both contributed to the psychopathology of this episode.

1. Introduction

Although the association between epilepsy and psychosis has been noted since the mid-nineteenth century, the role of seizures in the pathogenesis of psychoses in patients with epilepsy and whether epileptic psychosis and endogenous psychosis, such as schizophrenia, are the same are unknown [1–3]. Psychoses, comorbid with epilepsy, are classified according to the temporal relationship between seizure and psychosis and according to the type of epilepsy. Many studies have focused on the heterogeneity of epileptic psychoses [4–7]. Postictal psychosis is a type of epileptic psychosis that presents within a week of a seizure or a cluster of seizures and is known to be associated with temporal lobe epilepsy (TLE); however, this condition is rare among patients with idiopathic generalized epilepsy (IGE) [4,5,8–11]. Previous studies have documented that affective changes are frequently observed during postictal psychoses [10–12], and a case–control study indicated that postictal psychoses have a greater number of mania-like symptoms rather than schizophrenia-like symptoms, whereas interictal psychoses have a greater number of schizophrenia-like symptoms [4]. Our case report describes the case of a patient who had IGE and experienced 4 episodes of schizophrenia-like interictal psychosis before the age of 41 years. He did not experience any seizures or psychotic episodes from the age of 41 years to 56 years. At the age of 56 years, he experienced a generalized tonic-clonic seizure, which was followed by acute psychosis during the postictal stage; the psychosis was characterized by both schizophrenia-like and mania-like symptoms. In light of these findings, we have reviewed the current literature on epilepsy and postictal psychoses.

2. Case report

Informed consent was obtained from the patient and his family for this case report, and details that might disclose the identity of the patient have been omitted. The patient was a right-handed 56-year-old man with a history of febrile seizures; his first generalized convulsion occurred at 7 years of age. Although phenobarbital was administered subsequently, he experienced generalized tonic-clonic seizures not accompanied by aura a few times a year. He was a good student in high school, and he majored in science from one of the most prestigious universities in Japan. In his early twenties, he gradually became

* Corresponding author at: Department of Psychiatry, National Center of Neurology and Psychiatry, National Center Hospital, 4-1-1, Ogawa-Higashi, Kodaira, Tokyo 187-8551, Japan. Fax: +81 42 344 6745.
E-mail address: sakakibara-tky@umin.ac.jp (E. Sakakibara).

1525-5050/$ – see front matter © 2012 Elsevier Inc. All rights reserved.
doi:10.1016/j.yebeh.2012.04.127

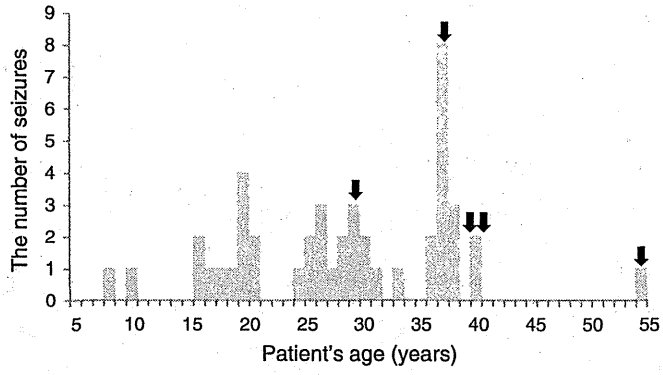

Fig. 1. Seizure frequency and psychotic episodes. Black arrows designate the episodes of psychosis.

suspicious that his seizures were the result of an assault by someone. After graduating from university, he became a high school teacher at the age of 26. At the age of 30 years, he experienced financial issues. While he was concerned with the dispute, his suspiciousness developed into a persecutory delusion that he had been attacked with high-frequency waves by an "offender;" consequently, he was hospitalized for 3 weeks at 31 years of age. The seizure frequencies are illustrated in Fig. 1.

After this first psychotic episode, he returned to work as a high school teacher and continued teaching until 38 years of age when a psychotic episode characterized by persecutory delusions, auditory hallucinations, including hearing the commanding voice of the "offender," and disorganized behavior occurred. He was unwilling to take antiepileptics. When the frequency of seizures reached as many as 8 per year, he was referred to an epilepsy center in Japan. Electroencephalogram (EEG) showed a very rare synchronized symmetrical bilateral diffuse spike-and-wave during the sleeping state (Fig. 2). His epilepsy was diagnosed as IGE on the basis of the clinical semiology of seizures and EEG findings. Subsequently, 400 mg/day of valproate and 4 mg/day of haloperidol were administered, which greatly reduced the frequency of seizures and resolved the psychosis. He experienced acute schizophrenia-like psychoses, characterized by delusion and hallucination, at the ages of 40 and 41; each episode remitted within 1 month without hospitalization. All these psychotic episodes occurred at >1-month interval from the nearest past seizures.

After the fourth psychotic episode, his seizures remitted and psychosis was not observed. He stopped working as a regular teacher at the age of 47 years and helped his family on their farm later; he did not marry. He has a strong family history of psychiatric illness among his first-degree relatives; his younger brother has epilepsy, acute transient psychosis, and mild retardation; his father was diagnosed with depression and committed suicide.

At the age of 56 years, he once attended to his mother overnight when she was sick. The next morning, he experienced a generalized tonic-clonic seizure for the first time in 15 years. On the next day, he began complaining about various somatic discomforts, including pain in his penis. He visited several physicians and surgeons, but no objective abnormalities were detected. Five days after the seizure, he began to hear the voice of the "offender," who directed him to "make emergency calls to police." His family witnessed his conversations with the voices. Because increasing the dosage of antipsychotics was ineffective, he was involuntarily hospitalized 21 days after the seizure. On admission, the patient was markedly elated, agitated, and talkative. Persecutory delusion, grandiose delusion, and conversations with voices were observed. He refused psychiatric examination and began shouting, for example, "I am the president of X University" and "I can receive air wave because the receiver has been implanted in my brain." He also complained that his penis was made painful by the "offender." Neurological examinations, laboratory data, computed tomography (CT), and magnetic resonance imaging (MRI) of the head showed no abnormality. EEG taken on admission showed 11 Hz, 50–100 μV, well-organized bi-occipital dominant α rhythm at rest with no paroxysmal discharge.

Treatment with intravenous haloperidol was initiated. By the third week of hospitalization, elated mood, agitation, pressured speech, and grandiose delusion had remitted; therefore, intravenous haloperidol was gradually replaced with oral haloperidol (~36 mg/day) and levomepromazine (~125 mg/day). By the seventh week of hospitalization, the auditory hallucinations and persecutory delusions had almost resolved. However, avolition and psychomotor inhibition became prominent, because of which the dosage of antipsychotics was changed to 4.5 mg/day of haloperidol and 125 mg/day of chlorpromazine. The patient was discharged 115 days after the admission. At the time of discharge, he had no current hallucinations or delusions, although he lacked insight that the voices he previously heard were hallucinations.

The Young Mania Rating Scale (YMRS) [13] and Positive and Negative Syndrome Scale (PANSS) [14] were evaluated weekly during the hospitalization. Fig. 3 illustrates the changes in YMRS scores and the positive and negative scales of PANSS. EEGs were performed repeatedly, but paroxysmal discharge was undetected. The results of the Wechsler Adult Intelligence Scale – Revised (WAIS-R) indicated borderline intelligence with significant decrease in performance intelligence quotient (IQ) relative to verbal IQ (full scale IQ, 80; verbal IQ, 92; performance IQ, 69).

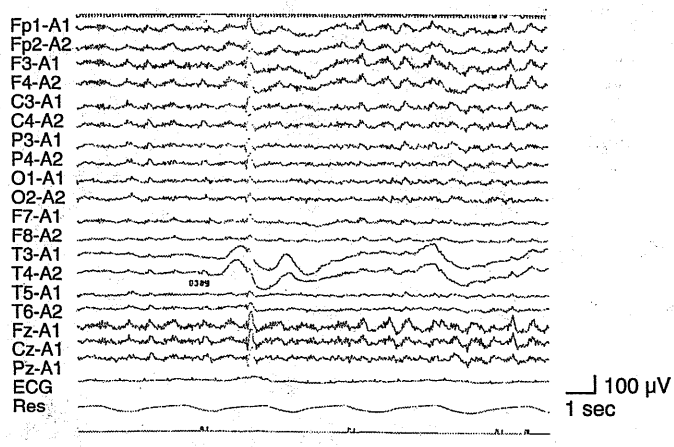

Fig. 2. An electroencephalogram taken at 39 years of age. Bilateral diffuse spike-and-wave was recorded.

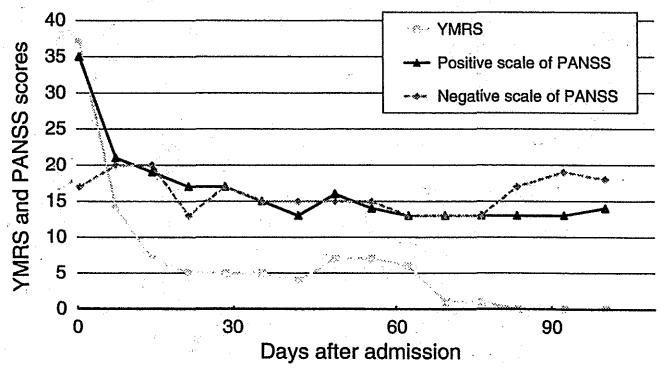

Fig. 3. Young Mania Rating Scale (YMRS) scores and positive and negative scale scores of Positive and Negative Syndrome Scale (PANSS) during hospitalization.

Table 1
Comparison of symptoms between interictal psychosis and postictal psychosis.
Adapted from [4,11,16,17].

	Postictal psychosis	Interictal psychosis	The present case
General feature	Mania-like	Schizophrenia-like	The mixture of both
Delusion	Grandiose, religious	Persecutory, referential	Grandiose, persecutory
First-rank symptoms	Rare	Common	Exist
Aggression, pressured speech, excessive emotional response	Common	Rare	Exist
Temporal relation to seizure	Mostly within 72 h after seizure	Unclear	Next day
Period of psychosis	Mostly within a month	Longer than postictal psychosis	2 months

3. Discussion

To understand the association between epilepsy and psychosis, both the specific type of epileptic syndrome and the temporal relationship between seizure and psychosis need to be considered.

3.1. Psychoses and specific epileptic syndromes

Psychoses are often seen among patients with localization-related epilepsy, especially TLE, which may be caused by dysfunctions of the temporal lobe and limbic system related to organic lesions and epileptic discharge [2]. On the other hand, psychoses are rarely seen in patients with IGE. A study reported that psychiatric symptoms were observed in 19.4% of 67 patients with IGE, most of which were episodic disturbances in behavior such as sexually aberrant activities; only 2 experienced auditory hallucinations and 1 experienced delusion [6]. Currently, there are no data on the correlation between IGE and schizophrenia-like psychosis. Adachi and colleagues found that the onset of psychosis in patients with generalized epilepsies is significantly earlier than that in patients with localization-related epilepsies (22.5 ± 1.0 years of age vs. 29.1 ± 0.7 years of age), and this onset is more comparable to what is seen in patients with schizophrenia [7]. Predisposed vulnerabilities to psychosis may contribute to the incidence of psychosis in patients with IGE, whereas epilepsy-related damage appears to be more relevant to psychoses in patients with localization-related epilepsy.

3.2. Interictal psychosis and postictal psychosis

The second important distinction to be considered is the temporal relationship between seizure and psychosis. Psychoses occurring in conjunction with or soon after a seizure or cluster of seizures indicate a positive relationship between seizure and psychosis. Another interesting case is alternating psychoses in which seizures and psychoses are observed in alternation [15]. When no such temporal link is observed, no direct relation is considered between seizures and psychoses.

Postictal psychosis was defined by Logsdail and Toone as a psychotic episode that occurs within a week of the last epileptic seizure and can last from 24 h to 3 months [8]. These authors excluded patients with a history of psychoses unassociated with seizures, and most subsequent studies on postictal psychosis have followed this definition of postictal psychosis [4,9,10,12]. Therefore, strictly speaking, the last episode of psychosis in the present case does not meet criteria for postictal psychosis as per this definition. However, it may be of some benefit to compare the present case with the examples of postictal psychoses documented in the literature. Adachi and colleagues have identified patients with epilepsy who have experienced acute psychoses during both the postictal and interictal periods [5,16] and have proposed the clinical entity of "bimodal psychosis" for this condition. The present case also comes under the parameters of bimodal psychosis.

Kanemoto and colleagues compared interictal psychosis and postictal psychosis among patients with TLE and noted differences in the symptoms of these 2 types of psychoses [4]. As shown in Table 1, interictal psychoses are more schizophrenia-like, in that first-rank symptoms (Schneider K) are more common and delusions are typically persecutory or referential. In contrast, postictal psychoses are more mania-like, where elated mood, aggression, pressured speech, and excessive emotional response are prominent and delusions are typically grandiose or religious. It is also known that seizures are sometimes followed by full-fledged manic episodes [18,19].

3.3. Postictal psychosis in IGE

Postictal psychoses are found more often in patients with localization-related epilepsy than in patients with IGE. The prevalence rates of postictal psychoses are reported to be from 3.7% [4] to 6.4% [12] in patients with TLE. Although rare, postictal psychoses have also been reported in patients with IGE [8,10,20].

When acute psychosis is observed during the postictal period in a patient with IGE, the question arises whether it is an epilepsy-related psychosis or a coincidence of endogenous psychosis. In the present case, the comorbidity of endogenous psychosis, especially schizophrenia, was suspected because there were 4 episodes of schizophrenia-like psychosis without noticeable temporal proximity to seizures. Evidence of family history of endogenous mental disorders and the apparent gradual decline in social functioning support this hypothesis. On the other hand, because the last psychotic episode began on the day following the seizure that had been dormant for 15 years, it is reasonable to assume that the seizure and the psychosis are related.

One hypothesis is as follows: The patient's family history indicated a predisposition to endogenous psychosis. When the patient was in his thirties and early forties, the propensity for psychosis was not sufficiently high and the seizures did not elicit psychoses. He experienced 4 seizure-unrelated psychotic episodes triggered by psychological burdens, such as financial issues and hardships experienced at work. After he stopped working as a teacher, the propensity for endogenous psychosis had not exceeded the threshold because he lived peacefully and did not experience seizures. However, he was getting progressively vulnerable to psychosis, as suggested by the decrease in IQ scores. At the age of 56 years, the patient's propensity for psychosis was sufficiently high for a seizure to trigger acute psychosis.

It is particularly noteworthy that the latest psychosis during the postictal period showed mania-like symptoms in addition to schizophrenia-like symptoms, whereas all the past 4 psychoses during the interictal periods showed schizophrenia-like symptoms without affective disturbance. This may suggest that both the predisposition to endogenous psychosis and the postictal neuronal process contributed to the psychopathology of the episode during the postictal period.

References

[1] Slater E, Beard AW. The schizophrenia-like psychoses of epilepsy. Br J Psychiatry 1963;109:95–150.
[2] Perez MM, Trimble MR. Epileptic psychosis — diagnostic comparison with process schizophrenia. Br J Psychiatry 1980;137:245–9.

[3] Sachdev P. Schizophrenia-like psychosis and epilepsy: the status of the association. Am J Psychiatry 1998;155:325–36.
[4] Kanemoto K, Kawasaki J, Kawai I. Postictal psychosis: a comparison with acute interictal and chronic psychoses. Epilepsia 1996;37:551–6.
[5] Adachi N, Matsuura M, Hara T, et al. Psychoses and epilepsy: are interictal and postictal psychoses distinct clinical entities? Epilepsia 2002;43:1574–82.
[6] Sengoku A, Toichi M, Murai T. Comparison of psychotic states in patients with idiopathic generalized epilepsy and temporal lobe epilepsy. Epilepsia 1997;38(Suppl. 6): 22–5.
[7] Adachi N, Akanuma N, Ito M, et al. Epileptic, organic and genetic vulnerabilities for timing of the development of interictal psychosis. Br J Psychiatry 2010;196: 212–6.
[8] Logsdail SJ, Toone BK. Postictal psychosis. A clinical and phenomenological description. Br J Psychiatry 1988;152:246–52.
[9] Savard G, Andermann F, Olivier A, Rémillard GM. Postictal psychosis after partial complex seizures: a multiple case study. Epilepsia 1991;32:25–31.
[10] Devinsky O, Abramson H, Alper K, et al. Postictal psychosis: a case control series of 20 patients and 150 controls. Epilepsy Res 1995;20:247–53.
[11] Trimble M, Kanner A, Schmitz B. Postictal psychosis. Epilepsy Behav 2010;19: 159–61.
[12] Kanner AM, Stagno S, Kotagal P, Morris H. Postictal psychiatric events during prolonged video-electroencephalographic monitoring studies. Arch Neurol 1996;53:258–63.
[13] Young RC, Biggs JT, Ziegler VE, Meyer DA. A rating scale for mania: reliability validity and sensitivity. Br J Psychiatry 1978;133:429–35.
[14] Kay SR, Flszbein A, Opfer LA. The positive and negative syndrome scale (PANSS) for schizophrenia. Schizophr Bull 1987;13:261–76.
[15] Wolf P. Acute behavioral symptomatology at disappearance of epileptiform EEG abnormality. Paradoxical or "forced" normalization. Adv Neurol 1991;55:127–42.
[16] Adachi N, Kato M, Sekimoto M, et al. Recurrent postictal psychosis after remission of interictal psychosis: further evidence of bimodal psychosis. Epilepsia 2003;44: 1218–22.
[17] Adachi N, Ito M, Kanemoto K, et al. Duration of postictal psychotic episodes. Epilepsia 2007;48:1531–7.
[18] Chakrabarti S, Aga VM, Singh R. Postictal mania following primary generalized seizures. Neurol India 1999;47:332–3.
[19] Nishida T, Kudo T, Inoue Y, et al. Postictal mania versus postictal psychosis: differences in clinical features, epileptogenic zone, and brain functional changes during postictal period. Epilepsia 2006;47:2104–14.
[20] Fong GC, Ho WY, Tsoi TH, Fong KY, Ho SL. Lateral temporal hyperperfusion in postictal psychosis assessed by 99mTc-HMPAO SPECT. Neuroimage 2002;17:1634–7.

指定発言：脳炎・脳症後てんかんの薬物治療

静岡てんかん・神経医療センター小児科 高橋幸利
静岡てんかん・神経医療センター神経内科 山崎悦子
北海道医療センター小児科 長尾雅悦
西新潟中央病院小児科 遠山 潤
名古屋医療センター神経内科 岡田 久
長良医療センター小児科 渡邊宏雄
宇多野病院小児神経科 白石一浩
南岡山医療センター神経内科 高田 裕
香川小児病院脳神経外科 夫 敬憲
呉医療センター小児科 宮河真一郎
三重中央医療センター小児科 田中滋己
神奈川病院小児科 四家達彦
長崎医療センター小児科 田中茂樹
長崎川棚医療センター神経内科 中根俊成
国立精神・神経医療研究センター病院小児神経科 佐久間啓
山形病院てんかんセンター神経内科 宇留野勝久

はじめに

急性脳炎・脳症は年間3100人程度発病していると思われ，半数以上に後遺症が残り，後遺症に対する治療・後遺症進行防止法の確立は重要な課題である．われわれは199症例の急性脳炎・脳症症例の後遺症を調査し，知的・運動障害は発病年齢が若いほど強く，てんかん発作・知的障害は慢性期に進行する経過を示すことを明らかにした[1]．次に，慢性期の抗グルタミン酸受容体(glutamate receptor；GluR)ε2抗体の有無と予後(ADL，てんかん発作，精神症状，知的障害，記憶障害，運動障害)との関係を，小児～成人の91症例で検討したところ，てんかん発作頻度・記憶障害の程度は抗GluRε2抗体陽性例で有意に重度であった．また，脳炎・脳症後てんかんではmatrix metalloproteinase-9(MMP-9)が高値で，血液脳関門が障害されていることを報告した(第43回日本てんかん学会)．脳炎・脳症後てんかんでは，通常のてんかん病態以外に抗GluRε2抗体，サイトカインや血液脳関門因子などが関与しているとわれわれは推定している．このような，特殊な病態も関与する脳炎・脳症後てんかん症例で，どのような抗てんかん薬が有効なのかを明らかにするための検討を行った．

1 対 象

国立病院機構政策医療ネットワーク共同研究(Ⅰ)急性脳炎・脳症後遺症治療と自己免疫病態研究班の参加施設等の急性脳炎・脳症後のてんかん症例109例(男性64例，女性45例)を対象とした．脳炎・脳症の原因は，単純ヘルペスウイルス1型(8例)，インフルエンザウイルス(6例)，細菌性髄膜脳炎(4例)，HHV 6(3例)，ワクチン関連脳症(3例)などである．脳炎の発病年齢(平均±SD)は9.1±11.7歳，てんか

ん発病年齢は10.1±11.8歳，解析対象抗てんかん薬開始年齢は16.6±15.9歳(中央値9.8歳)であった．

2 方 法

抗てんかん薬を増量していく過程で発作頻度を記録し，発作減少率(=[投与前発作頻度−投与後発作頻度]/投与前発作頻度)を4週間ごとに計算した．通院間隔が症例によって異なり，発作頻度が不明の期間もあるため，評価できた症例数は投与中の全例ではなかった．また，投与後期間が経つにつれ中止例，経過観察困難化もあり，評価可能症例数は減少した．発作完全抑制率(seizure free ratio；SFR)は発作が完全に抑制された(発作減少率=1.0)の症例の頻度を示し，>50％発作抑制率(responder rate；RR)は発作が半分以下に減った症例の頻度を示し，>50％発作悪化率(aggravation rate；AR)は発作が150％以上に増加した症例の頻度を示す．中止率(discontinuation ratio；DR)は，観察時に投与中止となった症例の頻度を示す．

3 結 果

109例のてんかん分類は症候性局在関連性てんかん99例，症候性全般てんかん8例，West症候群2例であった．併用抗てんかん薬は1.8±1.0剤で，バルプ

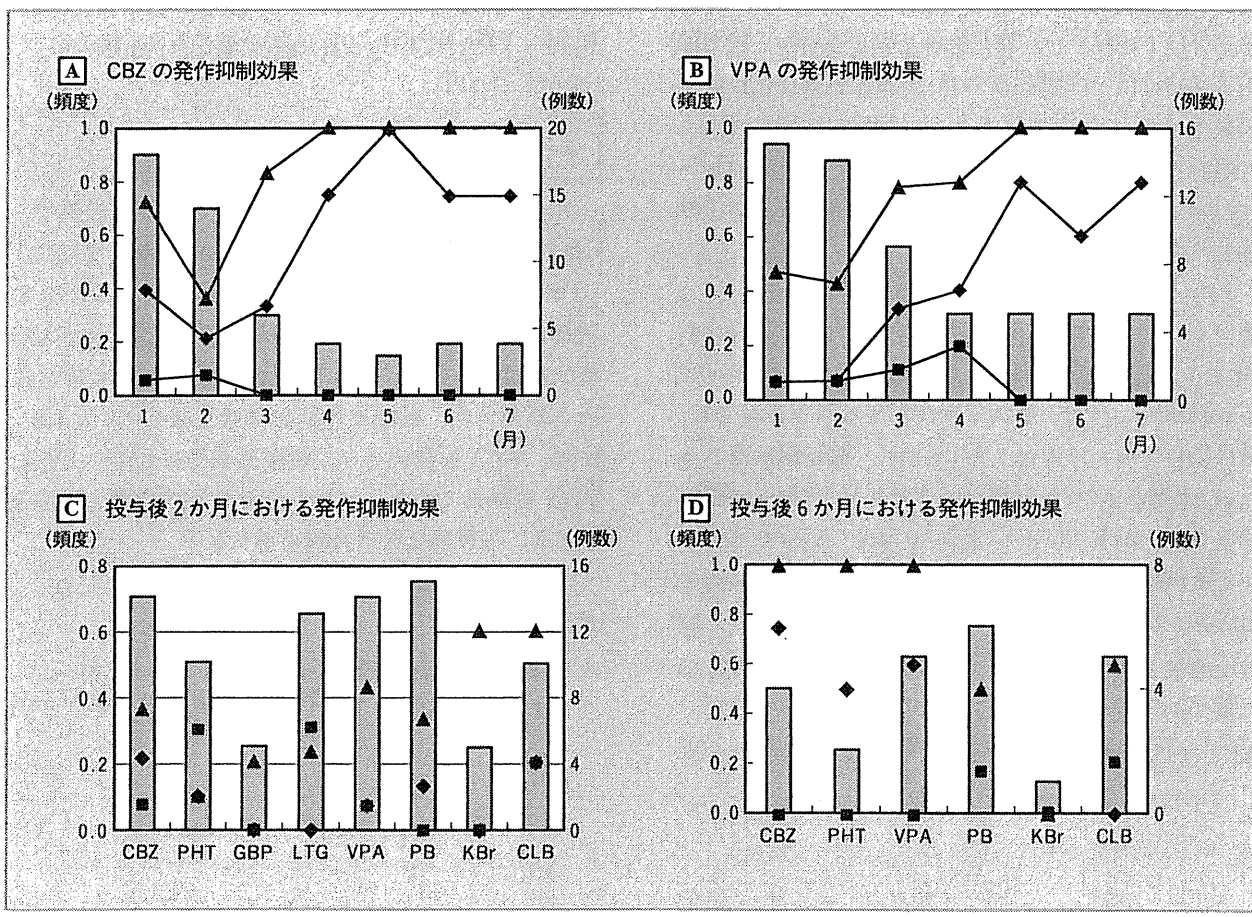

図1 発作抑制効果

棒グラフは症例数を，◆は発作完全抑制率を，▲は>50％発作抑制率を，■は発作悪化率を示す．

ロ酸ナトリウム(sodium valproate；VPA)，カルバマゼピン(carbamazepine；CBZ)，フェノバルビター ル(phenobarbital；PB)，フェニトイン(phenytoin；PHT)などの併用が多かった．発作頻度は，日単位55例，週単位38例，月単位8例，年単位7例であった(1例は不明)．症候性局在関連性てんかん症例の部分発作について，CBZは21例で検討した．投与開始後1か月(0～3週のあいだ)の発作頻度は18例で評価，SFR＝0.389，RR＝0.722，AR＝0.056と約40％の症例で発作が完全抑制され，70％の症例で発作が半分以下に減少し，悪化例は5％と少なかった(図1A)．投与開始後2か月(4～7週のあいだ)の発作頻度変化は症例が減り14例での評価であるが，SFR＝0.214，RR＝0.357，AR＝0.071と約20％の症例で発作が完全抑制され，35％の症例で発作が半分以下に減少し，悪化例は7％であった．投与開始後3か月(8～11週のあいだ)の発作頻度変化は症例が減り6例での評価であるが，SFR＝0.333，RR＝0.833，AR＝0と約30％の症例で発作が完全抑制され，80％の症例で発作が半分以下に減少し，悪化例はなかった．

VPAは16例で検討した．投与開始後1か月(0～3週のあいだ)の発作頻度は15例で評価，SFR＝0.067，RR＝0.467，AR＝0.067と約5％の症例で発作が完全抑制され，45％の症例で発作が半分以下に減少し，悪化例は5％と少なかった(図1B)．投与開始後2か月(4～7週のあいだ)の発作頻度変化は14例での評価であるが，SFR＝0.071，RR＝0.429，AR＝0.071と約5％の症例で発作が完全抑制され，40％の症例で発作が半分以下に減少し，悪化例は7％であった．投与開始後3か月(8～11週のあいだ)の発作頻度変化は9例での評価であるが，SFR＝0.333，RR＝0.778，AR＝0.111と約30％の症例で発作が完全抑制され，80％の症例で発作が半分以下に減少し，悪化例は10％であった．

投与後2か月(4～7週)における発作抑制効果を各抗てんかん薬で比較すると，SFRはCBZ＞クロバザム(clobazam；CLB)＞PB＞PHT＞VPAの順で，RRはCLB＞臭化カリウム(potassium bromide；KBr)＞VPA＞CBZの順であった．発作悪化は，ラモトリギン(lamotrigine；LTG)(30.8％)＞PHT(30.0％)＞CLB(22.2％)にみられた(図1C)．

長期効果として，6か月時の中止率はどの抗てんかん薬も60％以上と高くガバペンチン(gabapentin；GBP)＝LTG(100％)＞トピラマート(topiramate；TPM)＞PHT＞KBrの順であった．無効・発作増悪・副作用などでの中止が脳炎後てんかんでは多い．SFRはCBZ＞VPA＞PHTの順で，RRはCBZ＝PHT＝VPA＞CLB＞PBの順であった(図1D)．

4 考 察

109例の脳炎後難治局在関連性てんかん症例で，CBZ，PHT，ゾニサミド(zonisamide；ZNS)，GBP，TPM，LTG，VPA，PB，KBr，CLBの有効性を後方視的に検討した．脳炎・脳症後てんかんは難治で，薬疹などの副作用が出やすく[2]，中止率が60％と高かった．短期発作抑制効果ではCBZ，CLB，KBr，VPAが優れるが，長期効果ではCBZ，VPA，PHTが優れていた．治験と異なり経過観察が不完全であり，今後さらなる検討を要する．

References

1) 高橋幸利ほか：*Neuroinfection* 14：106-112, 2009
2) Mogami Y et al：*Brain Dev*：2011, Epub ahead of print

〈シンポジウムⅣ〉急性脳炎脳症

脳症の臨床特徴・自己抗体（抗グルタミン酸受容体抗体）：小児科領域

高橋幸利[1,2]、高久保瞳[1]、西村成子[1]、高尾恵美子[1]、笠井理沙[1]、那須裕郷[1]、山口解冬[1]

【要旨】小児期脳症での抗NMDA型GluR抗体の関与を検討するために、2相性脳症（AESD）、痙攣重積で発病し単相性の経過をとる脳症（SCSE）、非ヘルペス性急性辺縁系脳炎（NHALE）について、臨床症状、髄液所見、抗NMDA型GluR抗体等を比較検討した。重積で発病する小児期脳症の中で、早期発病のAESDでは抗NMDA型GluR抗体の関与は急性期に見られないが、幼児期発病のSCSEでは抗NMDA型GluR抗体の関与する症例の存在が示唆された。抗NMDA型GluR抗体を主体とするT細胞依存性の免疫介在性病態は年齢依存性があり、AESDの好発年齢帯の2歳前後では生じにくい、あるいは他の病態が先に起こる可能性がある。

Key words: NMDA型グルタミン酸受容体（NMDA-type Glutamate receptor）, GluR ε2 (NR2B), GluR ζ1 (NR1), 非ヘルペス性急性辺縁系脳炎（non-herpetic acute limbic encephalitis）, 痙攣重積型脳症

【1次性脳炎・2次性脳炎】

小児の脳炎・脳症は、代謝異常によるものもあるが、多くは感染を契機として発病する。感染に関係する急性脳炎・脳症はさらに、ウィルスの中枢神経系への直接侵達による狭義の脳炎＝1次性脳炎（ヘルペス脳炎など）[1]と、気道感染等に伴って駆動された免疫反応によって脳炎症状が起こる2次性脳炎（脳症）に分類される（表1）[2]。2次性脳炎（脳症）は、ウィルス感染時（あるいはその直後）に脳炎症状を示すが、髄液中のウィルスPCR検査あるいは剖検脳組織解析によりウィルスの中枢神経系直接浸達が否定される症例である。

【免疫応答と脳炎】

ウィルス感染で先ず始めに駆動される免疫は自然免疫（先天免疫）（innate immunity）で、マクロファージなどの食細胞、Natural killer cell(NK 細胞)、補体などが中心的役割を担っていて、感染局所で抗原非特異的に働いている（図1）。侵入したウィルスのDNAなどはToll like receptor 9 (TLR9)に、ウィルス膜タンパクはTLR4に結合し自然免疫が駆動され、抗ウィルス作用のあるⅠ型インターフェロン（IFN-α、IFN-β）や、炎症性サイトカインのTumor necrosis factor α (TNF α)などの分泌が誘導される。マクロファージの分泌するIL-12はNK細胞を活性化し、細胞傷害性T細胞と同じような機序で感染細胞をアポトーシスに導き、TNF αは血管内皮を活性化したり発熱をもたらしたりする。TNF αにより感染局所のリンパ流が増大すると、抗原と抗原提示細胞である樹状細胞がリンパ流に乗ってリンパ組織に到達、抗原特異的ナイーブT細胞をエフェクター化し、獲得免疫が駆動される。抗原特異的エフェクターT細胞は抗原特異的B細胞を活性化し、抗体産生を誘導する。

感染免疫の関与が示唆される2次性脳炎（脳症）をその発病ステージと症状で分類すると、①発熱などの感染症状とほぼ同時に脳炎症状が出現するもの（インフルエンザ脳症など）、②発熱などの感染症状

1：独立行政法人国立病院機構　静岡てんかん・神経医療センター（〒420-8688　静岡県静岡市葵区漆山886番地）　2：岐阜大学医学部小児病態学

とほぼ同時に痙攣重積で発病し、その後数日して発作が群発しbright tree appearanceと言われるMRI所見を呈する痙攣重積型脳症（2相性脳症、AESD, Acute encephalopathy with prolonged febrile seizures and late reduced diffusion）[3]、③発熱などの感染症状出現から数日後痙攣重積で発病するもの、④発熱などの感染症状出現から約1週間後辺縁系症状で発病するもの（非ヘルペス性急性辺縁系脳炎（non-herpetic acute limbic encephalitis, NHALE）など）、⑤感染終息後潜伏感染し、何年も経ってから再活性化により脳炎症状が出現するもの（幹細胞移植後辺縁系脳炎など）などが知られている（図1、表1）[2]。①②の感染症状とほぼ同時に脳炎症状が出現するものは、時期的には自然免疫の作

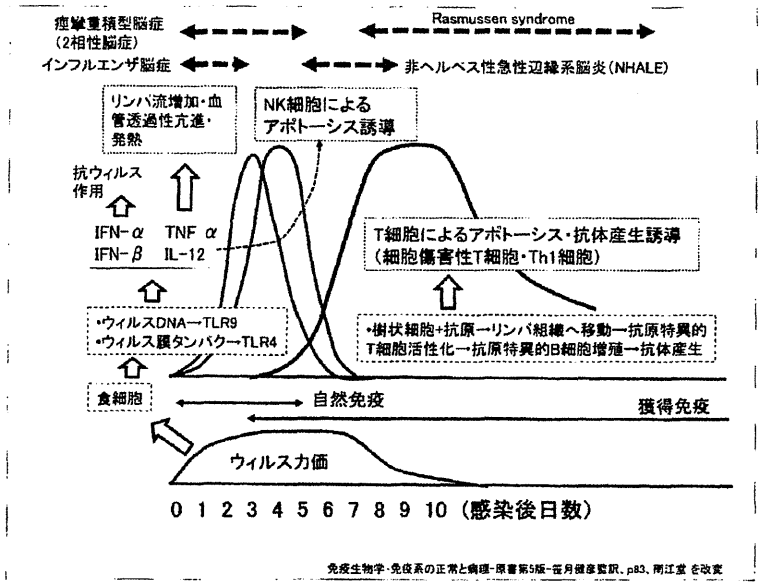

図1　ウィルス感染免疫と脳炎・脳症

ウィルス感染後に駆動される免疫機構を示す。NK細胞、Natural killer cell;TLR、Toll like receptor;IFN、インターフェロン;TNF α、Tumor necrosis factor α;IL-12、interleukin-12、AESD, Acute encephalopathy with prolonged febrile seizures and late reduced diffusion.

表1　脳炎の病態分類と原因ウィルス・脳炎診断

分類	原因ウィルス・脳炎診断
1次性脳炎	
1. 血行感染	● ムンプス・ポリオ・エンテロウィルスなど ● HSV(新生児)
2. 末梢神経を上行	● HSV・VZV・狂犬病ウィルスなど
2次性脳炎	
1. サイトカインによる障害	● インフルエンザ脳症 ● HIV脳症など ● 2相性脳症（痙攣重積型脳症）？
2. 細胞表面抗原に対する自己抗体による障害	● 非ヘルペス性急性辺縁系脳炎（抗NMDA型GluR抗体、抗VGKC関連蛋白抗体など）VGKC関連蛋白：LGI-1、CASPR2など ● 卵巣奇形腫合併急性辺縁系脳炎（抗NMDA型GluR抗体など） ● Bickerstaff型脳幹脳炎（抗GQ1b抗体など） ● 傍腫瘍性辺縁系脳炎（抗AMPA型GluR抗体、抗VGKC関連蛋白抗体など） ● 橋本脳症（抗NAE抗体など）
3. 細胞内抗原に対する自己抗体による障害？	● 傍腫瘍性辺縁系脳炎（抗Hu抗体など）？
4. 細胞傷害性T細胞による障害	● Rasmussen症候群、傍腫瘍性辺縁系脳炎？
5. 不明、その他	● ADEM

HSV, Herpes simplex virus; VZV, Varicella zoster virus; HIV, Human immunodeficiency virus; NMDA, *N*-methyl-D-aspartic acid; GluR, glutamate receptor; NAE, N-terminal of α-enolase; AMPA, α-amino-3-hydroxyl-5-methyl-4-isoxazole-propionate; ADEM, Acute disseminated encephalomyelitis.

用する時期の発病であり、TNFαなどのマクロファージ産生サイトカインやNK細胞の発病への関与が想定される。③ではNK細胞に加えてT細胞依存的な獲得免疫が駆動される時期であり、抗原特異的T細胞や特異抗体も関与する可能性がある。④のNHALEではT細胞依存的な獲得免疫が駆動される時期であり、NMDA型グルタミン酸受容体に対する抗体の関与が報告されている[4-6]。

【グルタミン酸受容体】

グルタミン酸受容体（GluR）は神経伝達物質であるグルタミン酸の受容体で、興奮性神経伝達に関与している。GluRにはイオンチャネル型と代謝型が存在、イオンチャネル型GluRは薬理学的にN-methyl-D-aspartate（NMDA）型とnon NMDA型に分類され、後者はalpha-amino-3-hydroxy-5-methyl-4-isoxazolepropionic acid（AMPA）型とカイニン酸型に分類される[7,8]。NMDA型GluRは、必須となるGluRζ1（NR1）と、GluRε1-4（NR2A－2D）あるいはGluRχ1-2（NR3A-3B）といったサブユニットが4つ会合した4量体（複合体）構造をとり、イオンチャネルとして機能しているが、種々のサブユニット会合パターンがあるとされている[5,9]。GluRの生理的機能は多岐に渡るが、中枢神経系疾患の病態にもGluRは深く関与している[5,10]。NMDA型GluRが中枢神経系疾患の病態に関与する機構には種々の病態が知られ、虚血性脳梗塞などに見られる①NMDA型GluRの興奮毒性による関与、てんかんなどで見られる②NMDA型GluR発現量変化による関与、NHALEなどに見られる③NMDA型GluRに対する自己抗体による関与、Rasmussen症候群などに見られるNMDA型GluRが④細胞傷害性T細胞のターゲットとなる場合などである[5]。

【抗NMDA型GluR抗体】

抗NMDA型GluR抗体は測定法により呼び方が異なり、サブユニットを抗原とする抗NR2B抗体（抗GluRε2抗体）（イムノブロット法、ELISA）、抗NR1抗体（抗GluRζ1抗体）（ELISA）と、NMDA型GluR複合体を抗原とする抗NMDAR抗体（抗NR複合体抗体）（cell-based assay）などがある。脳炎の抗NMDA型GluR複合体抗体は、シナプスなどのNMDAR複合体を細胞内へ内在化させることが分かっていて[11]、我々の研究ではNR1+NR2Bからなる NMDA型GluR複合体のみならずNR1単独のNMDA型GluRもNHALE患者の血清で内在化が起こる[12]。NMDA型GluR内在化は37度では起こるが4度では起こらない温度依存性の特徴を有している[12]。抗NMDA型GluR抗体はこのように、抗NMDA型GluRを内在化させることにより、NMDA型GluR拮抗作用を示し、辺縁系症状、アポトーシス抑制などに関与する（図2）[13]。

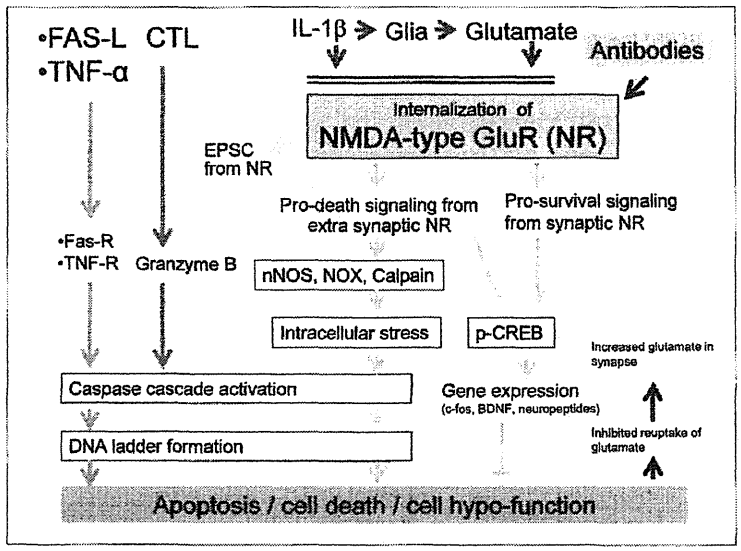

図2　NMDA型GluRを中心とした細胞死、細胞機能障害のメカニズム

FAS-L, FAS ligand; FAS-R, FAS receptor; TNF-α, Tumor Necrosis Factor-α; TNF-R, Tumor Necrosis Factor receptor; CTL, cytotoxic T cell; EPSC, excitatory postsynaptic current; nNOS, neuronal nitric oxide synthase; NOX, nitrogen oxide; p-CREB, phosphorylated cAMP-Responsive-Element-Binding protein; BDNF, Brain-derived neurotrophic factor.

【小児期脳症の臨床特徴と抗NMDA型GluR抗体】

小児期の脳症には様々な臨床型があり、種々の観点から命名、分類されている。病原体からの命名（インフルエンザ脳症など）、発病症状からの命名（NHALEなど）、臨床画像からの命名（AESDなど）、臨床経過からの命名（AERRPS, acute encephalitis with refractory, repetitive partial seizuresなど）、自己抗体からの命名（抗NMDAR脳炎など）などがあって、体系的な分類は難しいのが現状で、未分類の脳症はかなり存在する。

今回、比較的臨床特徴がまとまる①痙攣重積（群発を含む）で発病し数日後に発作が群発する2相性脳症（AESD）（20例）、②痙攣重積（群発を含む）で発病し単相性の経過をとる脳症（SCSE）（インフルエンザに伴う症例などを除く）（23例）、③小児期に辺縁系症状で発病したNHALE（36例）について、臨床症状、髄液所見、抗NMDA型GluR抗体等を比較検討し、小児期脳症の臨床特徴と抗NMDA型GluR抗体の関与を考察した（図3）。

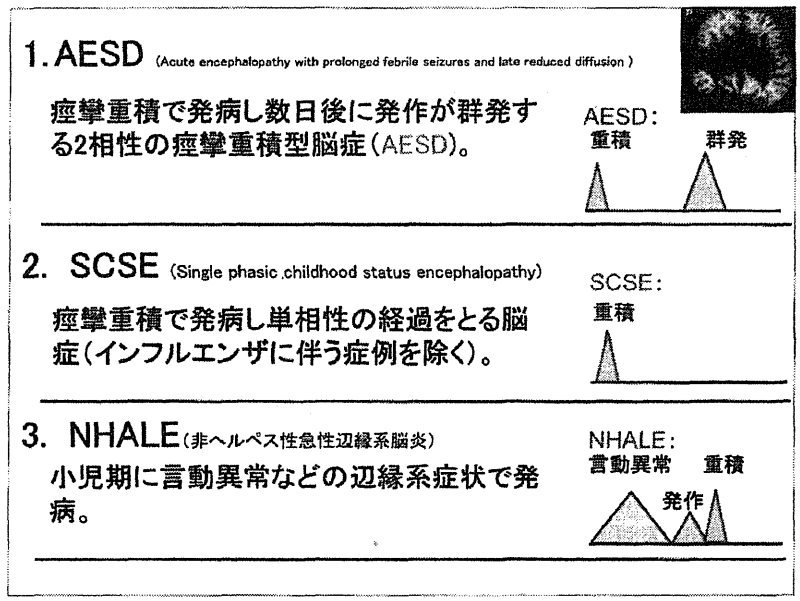

図3　小児期の急性脳症と臨床経過
検討した小児期脳症の3病型の臨床特徴を示す。

1．臨床特徴

発病年齢（平均±SD）はAESD（2.3±1.8歳）<SCSE（6.6±4.0歳）<NHALE（9.5±3.6歳）の順で、AESDはSCSE、NHALEより有意に低年齢発病で（Mann Whitney test, $p<0.0001$）、SCSEはNHALEより有意に低年齢発病であった（Mann Whitney test, $p<0.009$）。SCSEではAESDに近い2-3歳の発病群とNHALEに近い10歳前後の群があった。

先行感染症のHHV6/7感染はAESDのみに見られ、NHALEでは先行感染症が認められない症例が、他の病型に比べて多かった。先行感染から神経症状出現までの日数（平均±SD）はAESD（0.9±1.3日）<SCSE（4.3±3.4日）<NHALE（6.0±4.0日）の順で、AESDはSCSE、NHALEより有意に日数が短かった（Mann Whitney test, $p<0.0001$）。SCSEではAESDに近い発熱1日後に重積で発病する症例と、発熱5日くらいのNHALEに近い経過で発病する症例が混在していた。

初発神経症状はAESDでは90％が重積で、10％が群発、SCSEでは61％が重積で、39％が群発であった。SCSEの中にはNHALEの特徴である辺縁系症状を痙攣重積後の急性期に示す症例が7/23（39％）と、AESD（15％）より多かった。

2．治療・予後

人工呼吸器はSCSE：10/23例、AESD：4/20例、NHALE：3/27例で発病から4日以内に使用され、パルス治療はAESD：12/17例、SCSE：17/22例、NHALE：13/22例で行われていた。ADL(Barthel score)はNHALEがAESDより有意によく（Mann Whitney test, $p=0.0004$）、認知機能予後もNHALEがAESDより有意によく（Mann Whitney test, $p=0.005$）、運動機能予後もNHALEがAESDより有意によく（Mann Whitney test, $p=0.007$）、急性期入院日数は